Article

Cancer Cell

RIPK3 Restricts Myeloid Leukemogenesis by Promoting Cell Death and Differentiation of Leukemia Initiating Cells

Graphical Abstract

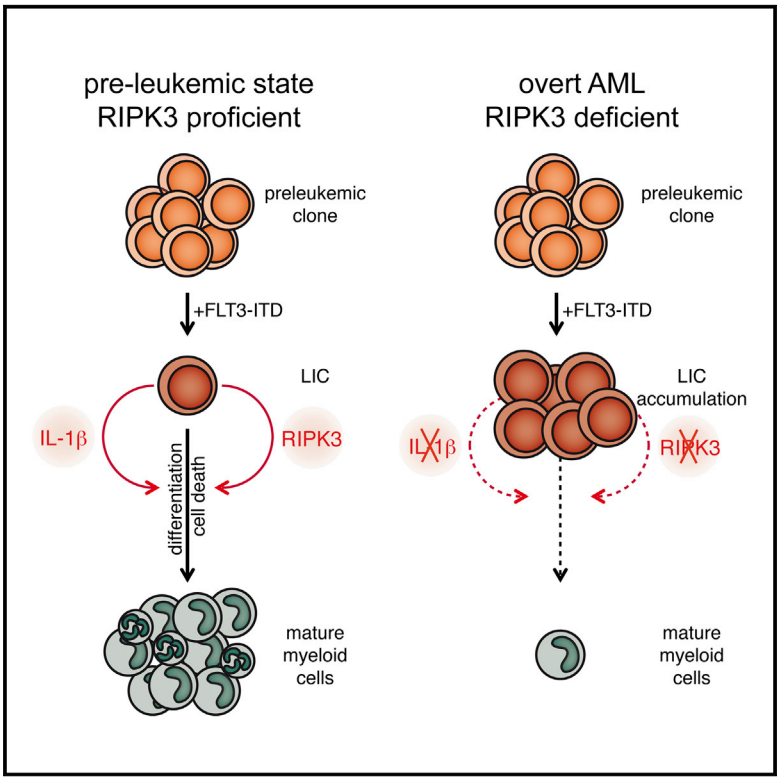

Highlights

- RIPK3 suppresses HSPC transformation by promoting cell death and differentiation
- Cell death in leukemia-initiating cells is driven by TNFR-driven RIPK3 activation
- RIPK3 promotes differentiation of LIC by activating the inflammasome
- RIPK3 expression is reduced in several subtypes of primary de novo AML

Authors

Ulrike Höckendorf, Monica Yabal, Tobias Herold, ..., Julia Slotta-Huspenina, Olaf Groß, Philipp J. Jost

Correspondence

philipp.jost@tum.de

In Brief

Höckendorf et al. demonstrate that RIPK3 restricts malignant myeloproliferation by activating the inflammasome, which promotes differentiation and cell death, and that loss of RIPK3 increases leukemic burden in mice. Reduced RIPK3 expression is observed across several human acute myeloid leukemia subtypes.

Accession Numbers

GSE79040

Höckendorf et al., 2016, Cancer Cell *30*, 75–91
July 11, 2016
http://dx.doi.org/10.1016/j.ccell.2016.06.002

Cancer Cell
Article

RIPK3 Restricts Myeloid Leukemogenesis by Promoting Cell Death and Differentiation of Leukemia Initiating Cells

Ulrike Höckendorf,[1,12] Monica Yabal,[1,12] Tobias Herold,[2] Enkhtsetseg Munkhbaatar,[1] Stephanie Rott,[1] Stefanie Jilg,[1] Johanna Kauschinger,[1] Giovanni Magnani,[3] Florian Reisinger,[4] Michael Heuser,[5] Hans Kreipe,[6] Karl Sotlar,[7] Thomas Engleitner,[8,9] Roland Rad,[8,9] Wilko Weichert,[9,10] Christian Peschel,[1,9] Jürgen Ruland,[3,9] Mathias Heikenwalder,[4,11] Karsten Spiekermann,[2,9] Julia Slotta-Huspenina,[10] Olaf Groß,[3] and Philipp J. Jost[1,9,*]
[1]III. Medical Department for Hematology and Oncology, Klinikum rechts der Isar, Technische Universität München, 81675 München, Germany
[2]Department of Internal Medicine 3, University Hospital Grosshadern, Ludwig-Maximilians-Universität (LMU), 81377 München, Germany
[3]Institute of Clinical Chemistry and Pathobiochemistry, Klinikum rechts der Isar, Technische Universität München, 81675 München, Germany
[4]Institute of Virology, Helmholtz Zentrum München für Gesundheit und Umwelt (HMGU), 85764 Neuherberg, Germany
[5]Department of Hematology, Hemostasis, Oncology and Stem Cell Transplantation, Hannover Medical School, 30625 Hannover, Germany
[6]Institute of Pathology, Hannover Medical School, 30625 Hannover, Germany
[7]Institute of Pathology, Ludwig-Maximilians-University (LMU), 80337 München, Germany
[8]II. Medical Department for Gastroentreology, Klinikum rechts der Isar, Technische Universität München, 81675 München, Germany
[9]German Cancer Consortium (DKTK), German Cancer Research Center (DKFZ), 69120 Heidelberg, Germany
[10]Institute of Pathology, Klinikum rechts der Isar, Technische Universität München, 81675 München, Germany
[11]Division of Chronic Inflammation and Cancer, German Cancer Research Center (DKFZ), 69120 Heidelberg, Germany
[12]Co-first author
*Correspondence: philipp.jost@tum.de
http://dx.doi.org/10.1016/j.ccell.2016.06.002

SUMMARY

Since acute myeloid leukemia (AML) is characterized by the blockade of hematopoietic differentiation and cell death, we interrogated RIPK3 signaling in AML development. Genetic loss of *Ripk3* converted murine FLT3-ITD-driven myeloproliferation into an overt AML by enhancing the accumulation of leukemia-initiating cells (LIC). Failed inflammasome activation and cell death mediated by tumor necrosis factor receptor caused this accumulation of LIC exemplified by accelerated leukemia onset in *Il1r1*$^{-/-}$, *Pycard*$^{-/-}$, and *Tnfr1/2*$^{-/-}$ mice. RIPK3 signaling was partly mediated by mixed lineage kinase domain-like. This link between suppression of RIPK3, failed interleukin-1β release, and blocked cell death was supported by significantly reduced RIPK3 in primary AML patient cohorts. Our data identify RIPK3 and the inflammasome as key tumor suppressors in AML.

INTRODUCTION

Acute myeloid leukemia (AML) represents a group of aggressive hematopoietic neoplasms originating from the myeloid progenitor compartment (Huntly and Gilliland, 2005). Many somatic mutations in AML patients result in blocked myeloid differentiation and increased self-renewal of hematopoietic stem and progenitor cells (HSPC) (Tenen, 2003). The acquisition of additional genetic aberrations within the pool of pre-leukemic HSPC eventually gives rise to leukemia-initiating cells (LIC) (Shlush et al., 2014; Vassiliou et al., 2011). One such example is FMS-like tyrosine kinase 3 (FLT3) mutations, which are found in 30%–40% of cytogenetically normal AML patients and define a poor prognostic subgroup. Specifically, the constitutively

Significance

Acute myeloid leukemia is sustained by a rare subpopulation of leukemia-initiating cells (LIC) characterized by their survival capacity and differentiation blockade. However, the molecular mechanisms that control LIC integrity remain incomplete. Our study demonstrates that RIPK3 forces a highly inflammatory form of cell death of LIC resulting in the release of cytokines that drive hematopoietic differentiation by paracrine/autocrine IL-1β signaling. RIPK3 thereby reduces the pool of LIC essentially demonstrating tumor-suppressive functions in AML. RIPK3 repression in several human AML subgroups, including *FLT3*-mutated patients, emphasizes the relevance of blocking this pathway for LIC integrity. In order to eradicate the pool of LIC, future concepts aiming at reinstating RIPK3 signaling might therefore harbor therapeutic potential in AML.

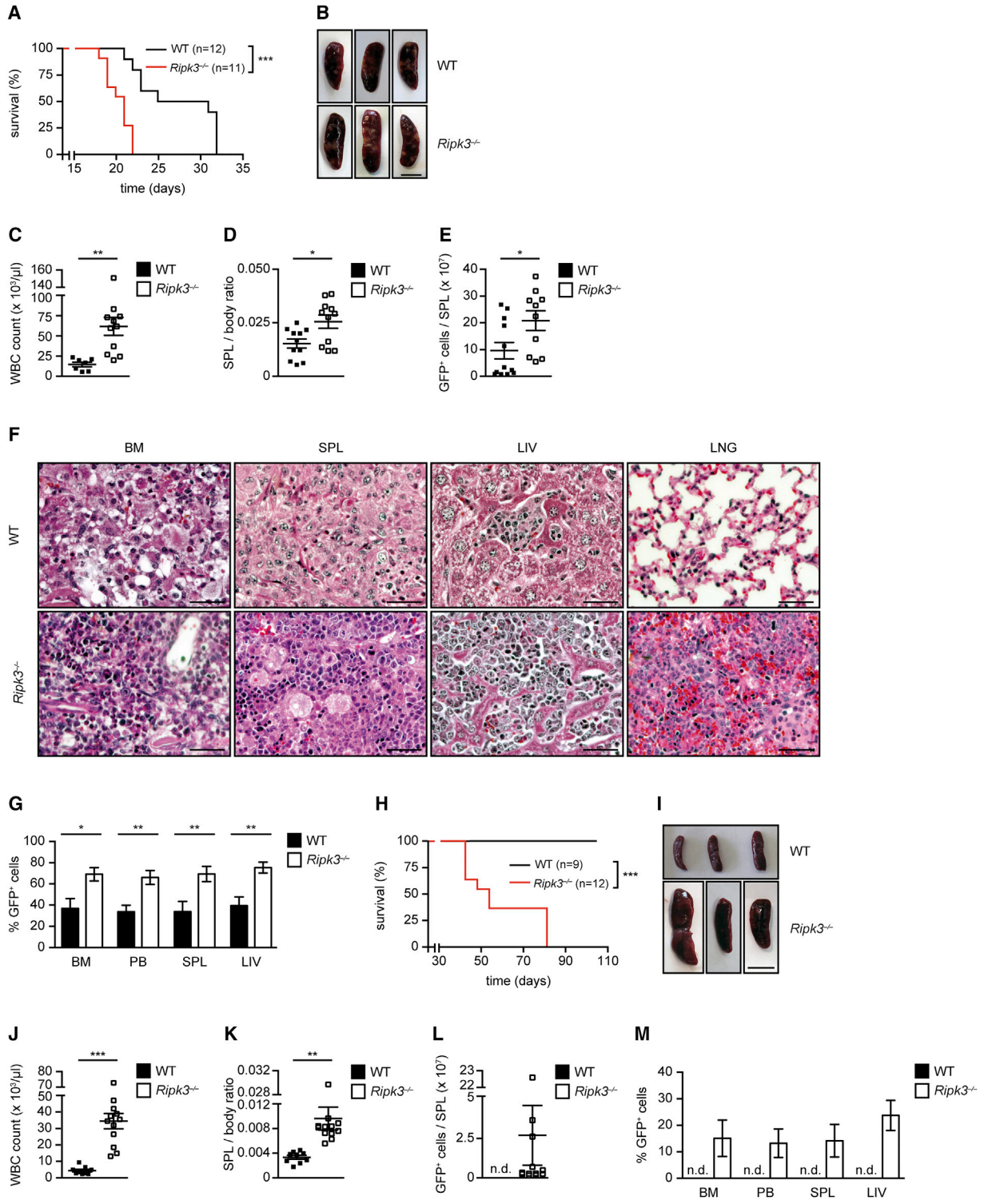

Figure 1. FLT3-ITD-Induced Myeloproliferation Is Accelerated in the Absence of *Ripk3* and Results in a Transplantable Leukemia

(A) Survival of WT mice transplanted with FLT3-ITD-transduced WT or *Ripk3*$^{-/-}$ BM. Median survival WT 28 days versus *Ripk3*$^{-/-}$ 21 days. Data are representative of two independent experiments.

(B) Spleens from mice in (A). Scale bar is 1 cm.

(C–E) Peripheral WBC counts (C), SPL/body ratio (D), and numbers of GFP^{+} cells per SPL (E).

(F) H&E staining of BM, SPL, LIV, and LNG collected from mice in (A). Scale bar is 40 µm.

(G) Frequency of GFP^{+} cells in the BM, PB, SPL, and LIV from mice in (A).

(legend continued on next page)

active FLT3-internal tandem duplication (FLT3-ITD) disrupts myeloid progenitor commitment and differentiation and promotes their expansion (Chu et al., 2012; Mead et al., 2013). One major obstacle to durable remissions in AML patients is the persistence of LIC after treatment (Shlush et al., 2014). Thus far, studies into cell death in AML have been focused on apoptosis, however the role of regulated necrosis (necroptosis) remains unclear (Vo et al., 2012).

Mature myeloid cells exhibit an exquisite propensity to activate receptor-interacting protein kinase 3 (RIPK3)-dependent cell death (Lawlor et al., 2015; Yabal et al., 2014). RIPK3 activation results in necroptotic cell death and the release of cytokines and danger-associated molecular pattern (DAMP) molecules (Pasparakis and Vandenabeele, 2015). Using murine models, RIPK3-dependent necroptosis has been shown to mediate severe disease pathology in the hematopoietic compartment (Duprez et al., 2011; Rickard et al., 2014; Yabal et al., 2014). Necroptosis is executed, at least in part, by oligomerization of mixed lineage kinase domain-like (MLKL) and subsequent plasma membrane rupture (Cai et al., 2014; Wang et al., 2014). RIPK3 itself is the target of several upstream activators, the most prominent being RIPK1 within the tumor necrosis factor receptor (TNFR) signaling pathway (Pasparakis and Vandenabeele, 2015). TNFR and RIPK3 signaling have both been implicated in normal and emergency myelopoiesis (Rickard et al., 2014; Wong et al., 2014), and both TNFR1 and TNFR2 restrict the self-renewal capacity of healthy HSPC in vivo (Pronk et al., 2011). However, the impact of RIPK3- and TNFR1/2-mediated necroptosis on malignant transformation remains unclear.

In contrast to apoptosis, necroptosis promotes inflammation by the release of substantial amounts of cytokines from dying cells including interleukin-1β (IL-1β) (Lawlor et al., 2015; Yabal et al., 2014). IL-1β is a key cytokine for differentiation of HSPC along the myeloid lineage (Jacobsen et al., 1994). IL-1β is translated as an inactive proform and requires processing into bioactive IL-1β by inflammasomes. The central components of inflammasomes are caspase-1 and Apoptosis-Associated Speck-Like Protein Containing A CARD (ASC; encoded by *Pycard*) (Schroder and Tschopp, 2010).

The concerted action of cytokines and growth factors controls the self-renewal and survival of HSPC (Takizawa et al., 2012). In the context of AML, LIC also appropriate these survival pathways (Tenen, 2003). Recent studies demonstrate that HSPC, and therefore also likely LIC, are potent cytokine secretors themselves and direct their own differentiation (Zhao et al., 2014).

Here we examined the role of RIPK3 in HSPC undergoing malignant transformation and specifically how RIPK3 signaling affects survival and differentiation within the myeloid lineage.

RESULTS

RIPK3 Restricts Malignant Myeloproliferation

We took advantage of the murine bone marrow transplantation model of the FLT3-ITD-driven myeloproliferative disorder in mice to investigate the role of RIPK3 in AML (Kelly et al., 2002). As previously reported, transplantation of FLT3-ITD-transduced wild-type (WT) bone marrow (BM) into lethally irradiated syngeneic WT recipient mice (abbreviated as WT FLT3-ITD) resulted in a rapid and fatal myeloproliferative neoplasm (MPN) characterized by peripheral leukocytosis, hepato-splenomegaly, and infiltration into the BM, spleen, and liver (Figures 1A–1E and S1A–S1D).

WT recipient mice transplanted with FLT3-ITD-transduced *Ripk3*$^{-/-}$ BM (abbreviated as *Ripk3*$^{-/-}$FLT3-ITD) succumbed significantly faster to an MPN compared with WT FLT3-ITD (Figure 1A), which was associated with substantially elevated white blood cell (WBC) counts in the peripheral blood and increased hepato-splenomegaly (Figures 1B–1E and S1A–S1D). Histological examination showed a greater infiltration of leukemic cells in the BM, spleen, liver, and lungs of mice transplanted with *Ripk3*$^{-/-}$FLT3-ITD compared with WT FLT3-ITD (Figures 1F and S1E). The elevated leukemic burden in *Ripk3*$^{-/-}$FLT3-ITD was confirmed by flow cytometry of GFP$^+$ cells (Figures 1G and S1D).

Of note, upon serial transplantation of splenocytes from diseased mice, only *Ripk3*$^{-/-}$FLT3-ITD, but not WT FLT3-ITD, reconstituted and gave rise to an overt leukemia in secondary recipients (Figure 1H). Leukocytosis and myeloid organ infiltration were detected only in *Ripk3*$^{-/-}$FLT3-ITD secondary transplants (Figures 1I–1L and S1F–S1I) as verified by flow cytometry (Figure 1M) and histology (Figure S1J).

Since FLT3-ITD-driven MPN in WT mice is not serially transplantable (Figure 1H) (Kelly et al., 2002), this finding illustrated the enhanced capability of transformed HSPC to survive and to propagate a myeloid neoplasm when *Ripk3* was deleted.

RIPK3 Promotes the Differentiation of Transformed Myeloid Progenitors

We characterized the composition of the HSPC compartment in FLT3-ITD-transplanted mice to determine the factors responsible for the aggravated disease of *Ripk3*$^{-/-}$FLT3-ITD (Figures S2A and S2B). Similar to human AML, characterized by an accumulation of primitive HSPC (Tenen, 2003), we found a significant expansion of FLT3-ITD-expressing lineage-negative (Lin$^-$) cells in all tested organs in *Ripk3*$^{-/-}$FLT3-ITD (BM: *Ripk3*$^{-/-}$ 6.7% ± 1.3% versus WT 2.2% ± 0.7%; p = 0.0067) (Figure 2A). Evaluation of the Lin$^-$Sca1$^+$c-Kit$^+$ compartment (containing long- and short-term HSC [LT- and ST-HSC] and multipotent progenitor cells [MPP]) in comparison with the myeloid progenitor populations (Lin$^-$Sca1$^-$c-Kit$^+$) (containing common myeloid progenitors [CMP], granulocyte-macrophage progenitors [GMP], and

(H) Survival of mice serially transplanted with GFP$^+$ splenocytes from primary FLT3-ITD-transplanted WT or *Ripk3*$^{-/-}$ mice. *Ripk3*$^{-/-}$ median survival 50 days. Data are representative of two independent experiments.

(I) Spleens from mice in (H). Scale bar is 1 cm.

(J–L) Peripheral WBC counts (J), SPL/body ratio (K), and numbers of GFP$^+$ cells per SPL (L) from mice in (H).

(M) Frequency of GFP$^+$ cells in the BM, PB, SPL, and LIV from mice in (H). n.d., not detectable.

BM, bone marrow; PB, peripheral blood; SPL, spleen; LIV, liver; LNG, lung. Each dot represents a mouse, and error bars represent means ± SEM. p Values (A) and (H) Mantel-Cox test, otherwise Student's t test. *p < 0.05, **p < 0.005, ***p < 0.0005. See also Figure S1.

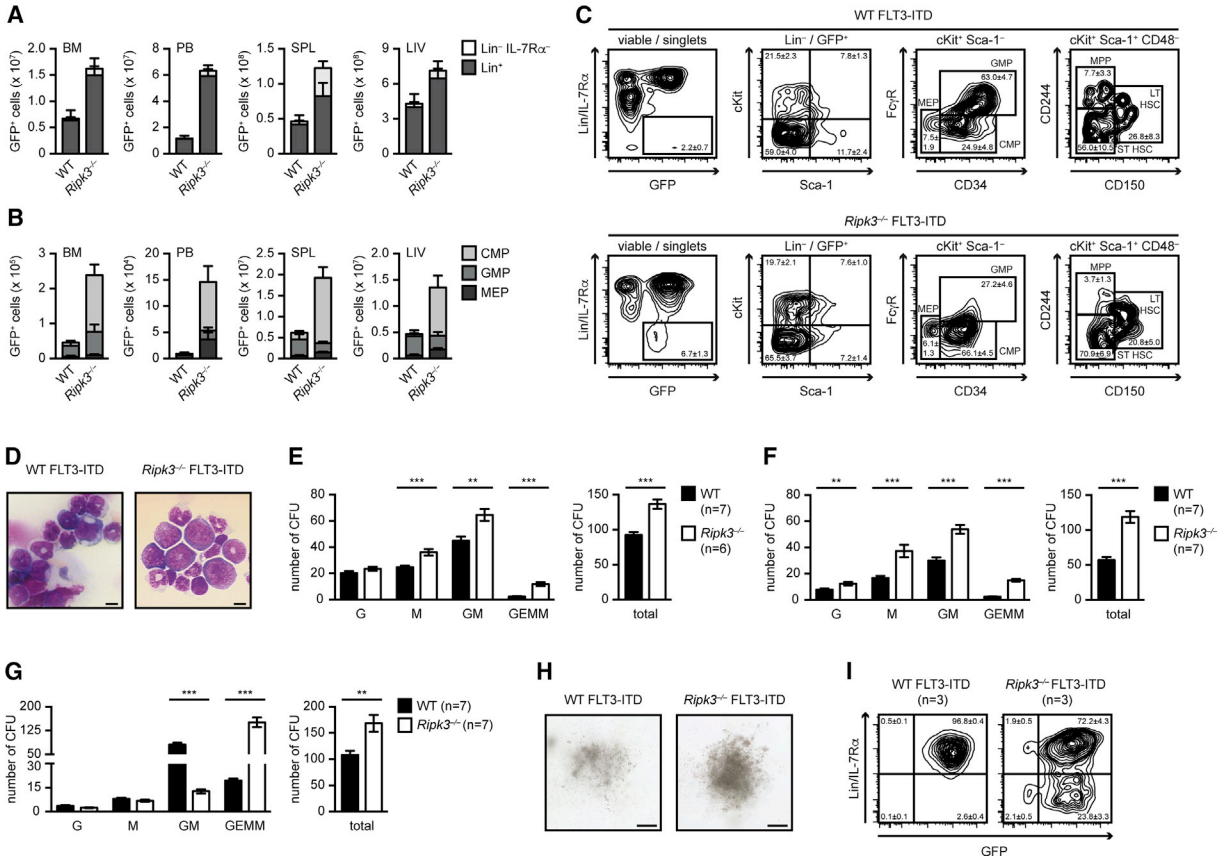

Figure 2. Accumulation of Malignant ST-HSC and CMP in *Ripk3*$^{-/-}$FLT3-ITD

(A and B) Absolute numbers of GFP$^+$ mature (Lin$^+$) cells and HSPC (Lin$^-$IL-7Rα$^-$) (A) and myeloid progenitor subsets (CMP, GMP, MEP) (B) in the BM (per hindlimb), PB, SPL, and LIV of WT and *Ripk3*$^{-/-}$FLT3-ITD burdened mice.

(C) Flow cytometric analysis of the BM from mice in (A). Numbers indicate percentage (±SEM). Data represent eight mice per genotype (A–C).

(D) Pappenheim stain of a BM cytospin collected from a *Ripk3*$^{-/-}$FLT3-ITD burdened mouse. Scale bar is 20 μm.

(E–G) Colony count of unchallenged (E), 5-FU-challenged (F), and FLT3-ITD-transduced (G) WT or *Ripk3*$^{-/-}$ BM. Shown are numbers of colony-forming units (CFU) of granulocyte (G), macrophage (M), granulocyte/macrophage (GM), and granulocyte/erythroid/macrophage/megakaryocyte (GEMM). Data are representative of at least three independent experiments.

(H) Representative pictures of FLT3-ITD-transduced WT and *Ripk3*$^{-/-}$ GEMM colonies. Scale bar is 300 μm.

(I) Flow cytometric analysis of in vitro cultures of FLT3-ITD-transduced WT or *Ripk3*$^{-/-}$ BM. Numbers in plots indicate percentage (±SEM). Data are representative of at least three independent experiments.

Error bars represent means ± SEM. p Values Student's t test: $^{**}p < 0.005$, $^{***}p < 0.0005$. See also Figure S2.

megakaryocyte-erythroid progenitors [MEP]) revealed that the expansion was mostly attributable to an increase in the CMP population (BM: *Ripk3*$^{-/-}$ 66.1% ± 4.5% versus WT 24.9% ± 4.8%; $p < 0.0001$) (Figures 2B, 2C, and S2C). Moreover, we observed a distinct increase in the ST-HSC population in *Ripk3*$^{-/-}$FLT3-ITD (BM: *Ripk3*$^{-/-}$ 70.9% ± 6.9% versus WT 56.0% ± 10.5%; Figures 2C and S2C). Together, the characterization of the HSPC compartment in burdened mice showed a marked shift toward more primitive multipotent CMP and ST-HSC only in *Ripk3*$^{-/-}$FLT3-ITD, while in WT FLT3-ITD the GMP compartment was expanded and the stem cell compartment was depleted as previously reported (Chu et al., 2012; Kelly et al., 2002). This was supported by the presence of leukemic blasts only in the BM of *Ripk3*$^{-/-}$FLT3-ITD (Figure 2D).

To exclude the possibility that the increased number of primitive progenitors in *Ripk3*$^{-/-}$FLT3-ITD might be explained by the inability of *Ripk3*$^{-/-}$ HSPC to differentiate into a specific myeloid lineage, we assayed their colony-forming capacity. BM from unchallenged or fluorouracil (5-FU)-challenged (HSPC-enriched) WT or *Ripk3*$^{-/-}$ mice showed normal differentiation into all myeloid lineages (Figures 2E and 2F). Although the distribution of myeloid lineages at steady state was similar to WT, the total number of colonies observed in unchallenged *Ripk3*$^{-/-}$ and HSPC-enriched *Ripk3*$^{-/-}$ BM was higher (Figures 2E and 2F). In line with previous reports, this did not translate into significant changes within the myeloid, lymphoid, or HSPC compartment of *Ripk3*$^{-/-}$ mice at steady state (data not shown) (Newton et al., 2004). Therefore, differentiation along the myeloid lineage at steady state was independent of RIPK3.

In contrast, oncogenic transformation of HSPC by FLT3-ITD resulted in the accumulation of myeloid progenitor populations in vitro (Figure 2G). Transformed *Ripk3*$^{-/-}$ HSPC remained

substantially more primitive as illustrated by the almost 10-fold increase in multipotent granulocyte/erythroid/macrophage/megakaryocyte (GEMM) colony numbers and the corresponding reduction in lineage-restricted granulocyte (G)/macrophage (M)/GM colonies (Figure 2G). This was in contrast to WT HSPC, which predominantly differentiated into lineage-committed GM colonies (Figure 2G). Morphologically, we observed that *Ripk3*$^{-/-}$ GEMM colonies were larger and denser compared with WT, suggestive of a failure to undergo cell death (Figure 2H). This was further supported by in vitro cultures of FLT3-ITD-transformed HSPC, which showed a considerable increase in Lin$^-$ cells in *Ripk3*$^{-/-}$, whereas WT differentiated largely into Lin$^+$ cells (Figure 2I).

In summary, the deletion of *Ripk3* resulted in a marked accumulation of leukemic CMP and ST-HSC in vivo and in vitro, a compartment known to contain LIC (Huntly and Gilliland, 2005). Thus, *Ripk3*$^{-/-}$FLT3-ITD was substantially more aggressive and led to the development of an overt transplantable AML.

TNFR Signaling Limits Leukemia Development

TNFR signaling is known to restrict HSPC numbers (Pronk et al., 2011; Volk et al., 2014) and to control RIPK3 activation. We therefore reconstituted WT recipients with FLT3-ITD-transduced *Tnfr1/2*$^{-/-}$ BM (*Tnfr1/2*$^{-/-}$FLT3-ITD) (Figure 3A). As observed for *Ripk3*$^{-/-}$FLT3-ITD, the transplantation led to a fatal MPN with elevated WBC counts and a reduced latency compared with control (Figures 3A and 3B). Despite only slight differences in clinical parameters, we observed a strong increase in the overall leukemic burden in mice with *Tnfr1/2*$^{-/-}$FLT3-ITD (Figures 3C and S3A–S3E). In marked similarity to *Ripk3*$^{-/-}$FLT3-ITD, Lin$^-$ cells represented a distinct population in *Tnfr1/2*$^{-/-}$FLT3-ITD (Figures 3C and 3D), with a substantial increase of the CMP and ST-HSC populations (BM: ST-HSC *Tnfr1/2*$^{-/-}$ 88.8% ± 4.4% versus *Ripk3*$^{-/-}$ 70.9% ± 6.9% versus WT 56.0% ± 10.5%; Figures 3E and S3F). Serial transplantations of *Tnfr1/2*$^{-/-}$ FLT3-ITD, but not of WT FLT3-ITD, led to a fully transplantable and fatal disease (Figures 3F, 3G, and S3G–S3N).

In vitro, *Tnfr1/2*$^{-/-}$FLT3-ITD cultures accumulated myeloid progenitors similar to what was observed in *Ripk3*$^{-/-}$FLT3-ITD (Figure 3H). Accordingly, in colony-forming unit (CFU) assays, *Tnfr1/2*$^{-/-}$ and *Ripk3*$^{-/-}$FLT3-ITD-transformed progenitors gave rise to significantly more multipotent GEMM colonies, and more colony numbers overall (Figure 3I). Thus, *Tnfr1/2*$^{-/-}$FLT3-ITD displayed features of an overt AML similar to *Ripk3*$^{-/-}$FLT3-ITD, both being characterized by elevated ST-HSC and CMP numbers. These data revealed the importance of TNFR signaling for restricting FLT3-ITD-transforming capacity in HSPC.

The major function ascribed to RIPK3 downstream of TNFR1 is to induce cell death. Here, the activation of RIPK3 is regulated by the ubiquitylation status of RIPK1, which is in turn controlled by the cellular inhibitor of apoptosis proteins 1 and 2 (cIAP1/2) (Bertrand et al., 2008). Fluorescence microscopy of FLT3-ITD-transduced WT progenitors grown in the presence of propidium iodide (PI) showed that GEMM colonies underwent cell death, as they became PI$^+$ during the cultivation period. In contrast, *Tnfr1/2*$^{-/-}$ and *Ripk3*$^{-/-}$ GEMM remained PI$^{-/lo}$ during the entire cultivation implying protection against cell death (Figure 3J). This is in line with the paradigm that cell death and proliferation together modulate hematopoietic colonies and contribute to the differentiation of HSPC and their progeny as they mature (Takizawa et al., 2012). Cell death was also inhibited by the RIPK1 kinase inhibitor Nec1s as WT FLT3-ITD GEMM remained PI$^{-/lo}$, and the number of total and GEMM colonies significantly increased upon this treatment (Figures 3J and 3K). In summary, cell death downstream of FLT3-ITD is inhibited by the genetic deletion of *Tnfr1/2*, *Ripk3,* or the pharmacologic inhibition of RIPK1.

Genetic Deletion of *Mlkl* Aggravates FLT3-ITD Leukemogenesis

To gain insight into how FLT3-ITD affects intracellular signaling networks within the HSPC compartment, we performed a global mRNA profiling analysis of fluorescence-activated cell sorting (FACS)-sorted murine FLT3-ITD Lin$^-$ cells compared with empty-vector controls at 48 hr post-infection. To identify gene sets specifically enriched in FLT3-ITD HSPC, we compared the average $\log_2$ mRNA microarray values with controls and identified 215 upregulated genes. Gene ontology analysis of the upregulated genes identified a strong correlation with inflammatory signaling as well as cytokine production and sensing (Figures 4A and S4A), as has been previously described in human FLT3-ITD AML (Cauchy et al., 2015).

RT-PCR of FLT3-ITD-transduced cultures and controls validated that the oncogene induced an inflammatory program (Figure 4B). The cytokines *Tnf* and *Il6,* the inflammasome components *Pycard* and *Casp1*, as well as *Ripk3*, were significantly upregulated (Figure 4B). In contrast, cIAP1 (*Birc2*), cIAP2 (*Birc3*), *Il1b*, and *Mlkl* expression were reduced (Figure 4B). These changes were confirmed by immunoblotting (Figure 4C) and indicated that TNFR1/2- and RIPK3-dependent signaling is activated by FLT3-ITD. This finding suggested that the reduced cIAP1/2 expression in concert with elevated expression of RIPK3 itself, effectively switches TNFR1 signaling toward cell death.

The reduced expression of *Mlkl* implied that suppression of cell death was beneficial for the survival of LIC. We therefore addressed the role of MLKL in FLT3-ITD leukemogenesis and tested whether deletion of *Mlkl* would affect disease progression. Transplantation of FLT3-ITD-transduced *Mlkl*$^{-/-}$ BM into WT recipients (*Mlkl*$^{-/-}$FLT3-ITD) led to similar overall survival and clinical parameters (Figures S4B–S4I) despite higher WBC counts and increased organ infiltration of GFP$^+$ cells compared with WT (Figures 4D and S4J). FACS analysis showed an accumulation of CMP and ST-HSC cells in *Mlkl*$^{-/-}$FLT3-ITD similar to *Ripk3*$^{-/-}$FLT3-ITD (Figures 4E–4G, S4K, and S4L). These data indicated that in vivo MLKL restricts leukemogenesis by promoting the differentiation of malignant HSPC similar to RIPK3.

In vitro, the survival advantage of Lin$^-$ *Mlkl*$^{-/-}$FLT3-ITD cells became apparent in colony assays and liquid cultures specifically within the CMP and ST-HSC compartments. Sorted ST-HSC from *Ripk3*$^{-/-}$ and *Mlkl*$^{-/-}$ produced more GEMM colonies than WT (Figure 4H), and both ST-HSC and CMP retained significantly more Lin$^-$ cells in liquid culture (Figure 4I), a phenotype observed only when purified progenitors were used for the experiment (Figures S4M and S4N). Protection from cell death in *Mlkl*$^{-/-}$ GEMM colonies was only partial since PI$^+$ cells were detectable in culture (Figure S4O), implicating a possible role for apoptotic cell death.

In summary, MLKL activity contributed to suppressing leukemogenesis by promoting LIC differentiation. Unlike RIPK3, the action of MLKL was restricted to the ST-HSC and CMP

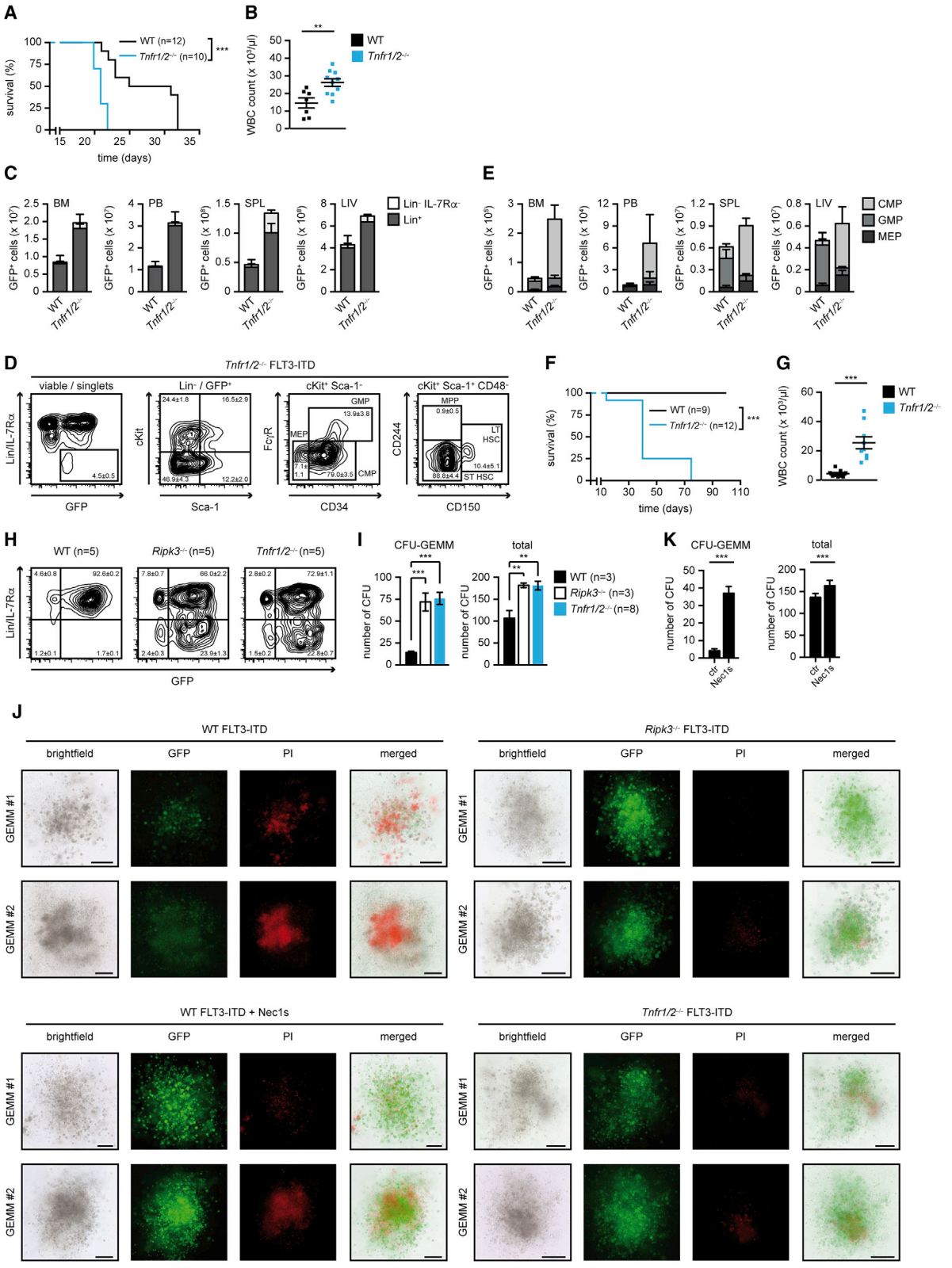

Figure 3. TNFR-Mediated RIPK1/RIPK3-Dependent Cell Death Restricts the Accumulation of Malignant Progenitors

(A) Survival of mice transplanted with FLT3-ITD-transduced WT or *Tnfr1/2*$^{-/-}$ BM. Median latency WT 28 days versus *Tnfr1/2*$^{-/-}$ 21 days. Data are representative of two independent experiments.

(legend continued on next page)

compartments, suggesting that additional effectors of RIPK3 contribute to the phenotype.

RIPK3 Controls Inflammasome Activation, which Promotes Differentiation of Leukemia-Initiating Cells

The strong cytokine signature observed in leukemic cells upon FLT3-ITD signaling (Figures 4A and S4A) prompted us to study the impact of RIPK3 on cytokines and LIC differentiation. We focused on IL-1β due to the increased expression of PYCARD and caspase-1 in FLT3-ITD-expressing cells (Figure 5A). Notably, we found that the cleaved active form of caspase-1 (p20), which processes IL-1β into its bioactive form, was only observed in WT FLT3-ITD cultures but not in *Ripk3*$^{-/-}$ (Figure 5A), suggesting that inflammasome activation occurred in a RIPK3-dependent manner.

To confirm that caspase activation occurred in LIC, we monitored caspase activation specifically within the Lin$^-$ population using a flow cytometry-based caspase inhibitor (Red-VAD-FMK), which detects cells harboring activated caspases by FACS. We observed a marked increase in caspase activation in WT Lin$^-$ cells upon FLT3-ITD signaling (Figure 5B), which could not be attributed to either caspase-8 (Figures S5A and S5B) or caspase-3 activation (data not shown). In contrast, caspase activation in *Ripk3*$^{-/-}$ or *Mlkl*$^{-/-}$ Lin$^-$ progenitors remained constant over time (Figure 5B) and correlated with an increase in cell numbers specifically of ST-HSC, suggesting reduced cell death or increased self-renewal (Figure S5C). As maturation into Lin$^+$ cells was unaffected in all three genotypes (Figure S5B), this pointed toward a cell intrinsic mechanism behind the elevated ST-HSC numbers in *Ripk3*$^{-/-}$ and *Mlkl*$^{-/-}$.

In line with this finding, significant amounts of IL-1β were detected in colony cultures of WT leukemic cells, but not in *Ripk3*$^{-/-}$, *Tnfr1/2*$^{-/-}$, and *Mlkl*$^{-/-}$ cultures (Figure 5C). As IL-1β is a potent inducer of myeloid differentiation, we tested whether addition of exogenous IL-1β in *Ripk3*$^{-/-}$ or *Tnfr1/2*$^{-/-}$ cultures was able to restrict the accumulation of LIC in culture. Indeed, colony assays and liquid cultures of *Ripk3*$^{-/-}$ or *Tnfr1/2*$^{-/-}$ FLT3-ITD cells differentiated normally when exogenous IL-1β was added, confirming that IL-1β was rate limiting for cellular differentiation of leukemic progenitors (Figures 5D, 5E, S5D, and S5E).

These data showed that FLT3-ITD signaling enhanced RIPK3-dependent inflammasome activity to produce IL-1β, thereby favoring myeloid differentiation, a process contributed to by TNFR and MLKL signaling. Blockade of these signaling pathways resulted in a differentiation failure within the HSPC compartment and subsequent accumulation of LIC, key drivers of leukemogenesis.

PYCARD and IL1R Suppress Leukemogenesis by Promoting Myeloid Differentiation

We transduced BM from IL1R1- or PYCARD-deficient mice with FLT3-ITD to further corroborate the role of IL-1β signaling in malignant myeloproliferation. FLT3-ITD expression in progenitors from *Il1r1*$^{-/-}$ or *Pycard*$^{-/-}$ mice induced a significant increase in Lin$^-$ cells and GEMM colonies (Figures 5F and 5G). Since processing and activation of IL-1β is carried out by caspase-1, or, alternatively, by caspase-8, we inhibited both enzymes pharmacologically in WT colony assays. Both inhibitors induced a significant increase in GEMM colonies consistent with caspase-1- and caspase-8-dependent IL-1β maturation (Figure 5H). Inhibition of IL-1R signaling itself using the IL-1R antagonist anakinra proved to be the most potent in blocking differentiation (Figure 5H). This implied that both the caspase-1- and caspase-8-dependent pathways of inflammasome activation promoted IL-1β signaling and subsequent differentiation of LIC.

We observed that the number of GEMM colonies in *Il1r1*$^{-/-}$ and *Pycard*$^{-/-}$ FLT3-ITD-transduced cultures were consistently less than that for *Ripk3*$^{-/-}$ (Figure 5G). We therefore examined whether RIPK1-dependent cell death was responsible for this difference. Indeed, blockade of RIPK1 by Nec1s further increased the number of *Il1r1*$^{-/-}$ GEMM colonies almost to the level observed in *Ripk3*$^{-/-}$ cultures (Figure 5I). Moreover, fluorescence microscopy of *Il1r1*$^{-/-}$ or *Pycard*$^{-/-}$ GEMM colonies showed reduced PI uptake upon culture with Nec1s indicative of reduced cell-death induction (Figure S5F), together showing that RIPK1-dependent cell death and IL-1β signaling both restrict LIC numbers in vitro.

We next examined the role of IL-1β in vivo by generating FLT3-ITD disease in *Ripk3*$^{-/-}$, *Il1r1*$^{-/-}$ (*Il1r1*$^{-/-}$FLT3-ITD), or *Pycard*$^{-/-}$ (*Pycard*$^{-/-}$FLT3-ITD) mice. The onset of the MPN in mice transplanted with *Il1r1*$^{-/-}$FLT3-ITD or *Pycard*$^{-/-}$FLT3-ITD was significantly faster compared with WT FLT3-ITD, and closely mimicked the disease observed in *Ripk3*$^{-/-}$FLT3-ITD (Figure 6A). Although WBC counts, clinical parameters, and organ infiltration

(B) Peripheral WBC counts from mice in (A).
(C) Absolute numbers of GFP$^+$ mature (Lin$^+$) cells and HSPC (Lin$^-$IL-7Rα$^-$) in the BM (per hindlimb), PB, SPL, and LIV of mice as in (A).
(D) Flow cytometric analysis of the BM from *Tnfr1/2*$^{-/-}$FLT3-ITD mice. Numbers indicate percentage (±SEM).
(E) Absolute numbers of GFP$^+$ myeloid progenitor subsets (CMP, GMP, MEP) in the BM (per hindlimb), PB, SPL, and LIV of mice as in (A). Data represent eight mice per genotype (C–E).
(F) Survival of mice serially transplanted with GFP$^+$ splenocytes from primary FLT3- ITD-transplanted WT or *Tnfr1/2*$^{-/-}$ mice. *Tnfr1/2*$^{-/-}$ median survival 40 days. Data are representative of two independent experiments.
(G) Peripheral WBC counts of mice in (F).
(H) Flow cytometric analysis of cultures of FLT3-ITD-transduced WT, *Ripk3*$^{-/-}$, and *Tnfr1/2*$^{-/-}$ BM. Numbers in plots indicate percentage (±SEM). Data are representative of two independent experiments.
(I) Colony count of FLT3-ITD-transduced WT, *Ripk3*$^{-/-}$, and *Tnfr1/2*$^{-/-}$ BM. Data are representative of four independent experiments.
(J) Fluorescence microscopic analyses of GFP expression and propidium iodide (PI) staining in CFU GEMM of FLT3-ITD-transduced WT (+/− Nec1s), *Ripk3*$^{-/-}$, and *Tnfr1/2*$^{-/-}$ BM. Scale bar is 300 μm. Data are representative of four independent experiments with at least six mice per genotype.
(K) Colony count of WT FLT3-ITD-transduced BM in the presence or absence of Nec1s. Data depict five mice and are representative of three independent experiments.
Each dot represents a mouse, and error bars represent means ± SEM. p Values (A) and (F) Mantel-Cox test, otherwise Student's t test: $^{**}p < 0.005$, $^{***}p < 0.0005$. See also Figure S3.

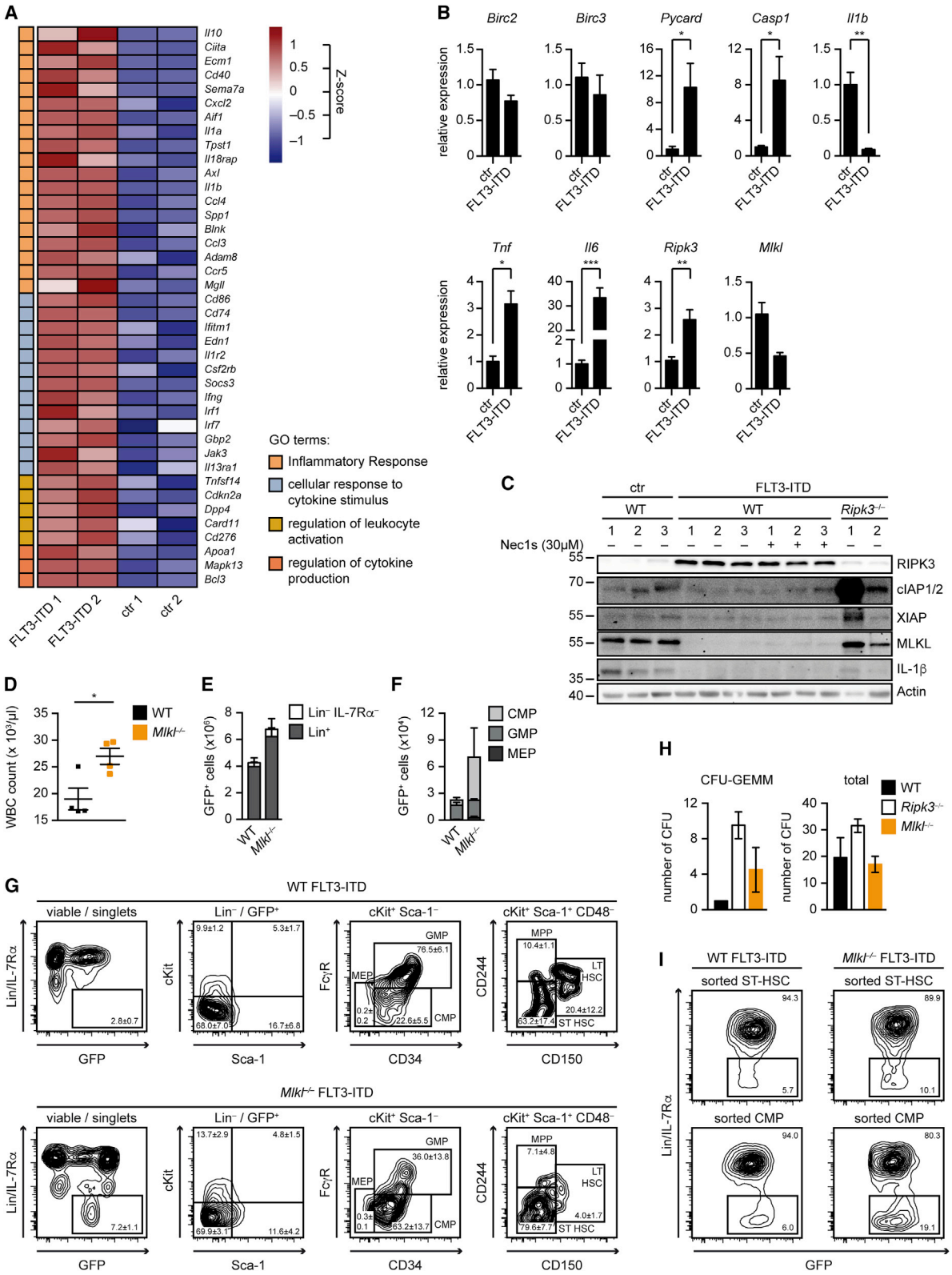

Figure 4. FLT3-ITD Leukemogenesis Is Aggravated by the Deletion of *Mlkl*

(A) Heatmap of gene ontology enrichment analysis comparing FACS-sorted murine FLT3-ITD Lin$^-$ cells compared with empty-vector controls (ctr) at 48 hr post-infection. The top 40 genes associated with an inflammatory cell signaling and $\log_2$ fold change >0.8 are shown, clustered by Gene Ontology terms. The color intensities indicate the Z score-transformed enrichment of each gene. Data represent one experiment with five mice.

(legend continued on next page)

in recipient mice transplanted with *Il1r1*$^{-/-}$FLT3-ITD or *Pycard*$^{-/-}$ FLT3-ITD were only slightly elevated compared with WT (Figures 6B and S6A–S6H), the same mice presented with a significant skewing of progenitor cells toward the CMP (BM: *Il1r1*$^{-/-}$ 55.5% ± 8.5%; *Pycard*$^{-/-}$ 60.7% ± 8.1%; WT: 12.5% ± 2.2%; p(WT versus *Il1r1*$^{-/-}$) = 0.0012; p(WT versus *Pycard*$^{-/-}$) = 0.0002) (Figures 6C, 6D, S6I, and S6J) and ST-HSC compartment (BM: *Il1r1*$^{-/-}$ 67.8% ± 10.9%; *Pycard*$^{-/-}$ 68.9% ± 10.9%; WT: 58.3% ± 16.4%; p(WT versus *Il1r1*$^{-/-}$) = 0.0562; p(WT versus *Pycard*$^{-/-}$) = 0.05) (Figures 6E and S6J). Serial transplantations of *Il1r1*$^{-/-}$FLT3-ITD and *Pycard*$^{-/-}$FLT3-ITD splenocytes led to leukemia and elevated WBC counts in recipient mice, albeit with a longer latency compared with *Ripk3*$^{-/-}$FLT3-ITD (Figures 6F and 6G). The survival data showed that impaired IL-1β signaling promoted FLT3-ITD leukemogenesis.

In summary, FLT3-ITD signaling promoted inflammasome activation, which limited the accumulation of LIC and subsequent leukemia development. Loss of *Ripk3* was, however, more potent in increasing the leukemic burden in mice, compared with the loss of *Il1r1* or *Pycard* alone, indicating that it is the dual control of cell death and IL-1β signaling that renders RIPK3 such a potent suppressor of leukemogenesis.

Expression of RIPK3 Is Reduced in Primary Human AML Samples

We interrogated two cohorts of 461 and 562 primary AML patient samples for mRNA expression of *RIPK3* and *MLKL* to validate the link between RIPK3 and tumor suppression in human AML (Herold et al., 2014; Verhaak et al., 2009). The datasets consisted of microarray analyses of newly diagnosed de novo AML patients. A significant reduction in *RIPK3* expression in several AML subgroups, including cytogenetically normal FLT3-ITD AML, was observed when compared with healthy bulk BM (FLT3-ITD 7.5 ± 0.1 versus healthy 7.9 ± 0.1; p = 0.0039; Figures 7A and 7B), as has been previously reported (Nugues et al., 2014). When compared with purified healthy HSC, *RIPK3* expression remained significantly reduced in FLT3-ITD AML in line with a significant role of RIPK3 for FLT3-ITD AML (Figures 7C and 7D). In addition, mRNA expression of *MLKL* within the same subgroup was also significantly reduced (FLT3-ITD 8.6 ± 0.2 versus healthy 9.5 ± 0.2; p = 0.0096; Figures S7A and S7B). The pattern of reduced *BIRC2* and *BIRC3* was also observed in this subset (Figure S7C). A comparison of gene expression data from AML with data from other MPN showed that the reduced expression of *RIPK3* and *MLKL* was unique to AML (Figures S7D–S7H).

Furthermore, several additional AML subtypes showed reduced *RIPK3* expression, supporting the notion that suppression of RIPK3-dependent cell death and differentiation in AML were not rare events. A notable exception was AML presenting with mixed lineage leukemia (*MLL*) gene translocations t(v;11)(v;q23) or t(9;11), which expressed *RIPK3* and *MLKL* at levels comparable with healthy individuals (Figures 7A, 7C, and S7A). This indicated that the suppression of RIPK3 signaling did not provide an advantage in this AML subtype.

To confirm that mRNA and protein levels correlated, we obtained primary human BM trephinations from a cohort of AML patients and performed immunohistochemistry for RIPK3 protein expression in comparison with healthy bone marrow. Indeed, RIPK3 expression was low to undetectable in blasts of CN-AML patients harboring *FLT3* mutations (either *FLT3-ITD* or *FLT3-TKD*) (Figure 7E). In line with the gene expression data, CN-AML patients with *FLT3* plus *NPM1* mutations showed low to intermediate RIPK3 protein expression in AML blasts (Figure 7F). In contrast, a strongly positive staining intensity for RIPK3 in AML patients harboring MLL translocations was observed, which correlated with the gene expression data (Figures 7A and 7B). This was similar to normal granulopoiesis and megakaryocytes, which also stained strongly positive for RIPK3, whereas erythropoiesis was mostly negative (Figure S7I). Immunoblotting of protein lysates of bone marrow aspirates from AML patients or healthy BM controls also confirmed the reduced expression of RIPK3 in several independent AML samples (Figure S7J).

In agreement with our mouse model, human *FLT3*-mutated leukemic blast cells exhibited reduced RIPK3 activity both on mRNA and on protein levels. The reduced expression of *RIPK3* in several AML subtypes supported the notion that suppression of RIPK3-dependent signaling in AML is positively selected for during leukemogenesis.

Acceleration of Leukemogenesis by RIPK3 Inhibition Is Not Restricted to FLT3-ITD-Mutated AML

To verify the tumor-suppressive function of RIPK3 in alternative AML subtypes, we transplanted WT mice with *Ripk3*$^{-/-}$ BM expressing the oncogenic fusion AML-ETO, which is caused by the frequent t(8;21) translocation (Yan et al., 2006), and has reduced *RIPK3* expression (Figures 7A, 7C, and 8A). Mice reconstituted with *Ripk3*$^{-/-}$AML-ETO succumbed substantially more rapidly to AML compared with WT (Figure 8B). The leukemic onset and the clinical parameters of WBC counts or leukemic burden in hematopoietic organs were accelerated by the genetic loss of *Ripk3* (Figures 8C and S8A–S8D). As described, AML-ETO induced the accumulation of FcγR$^{lo/med}$ CD34^{-} progenitors in both WT and *Ripk3*$^{-/-}$ (Yan et al., 2006) (Figures 8D–8F).

(B) Relative gene expression of 5-FU-enriched HSPC (ctr) compared with FLT3-ITD transduced WT BM. Data are representative of 5–12 biological repeats.
(C) Immunoblots of three samples each of 5-FU-enriched HSPC (ctr) or FLT3-ITD-transduced WT and *Ripk3*$^{-/-}$ BM cultured in the presence or absence of Nec1s (30 μM) for 7 days. Data are representative of three independent experiments.
(D) Peripheral WBC counts from mice transplanted with FLT3-ITD-transduced WT or *Mlkl*$^{-/-}$ BM.
(E and F) Absolute numbers of GFP^{+} mature (Lin^{+}) and HSPC (Lin^{-} IL-7Rα^{-}) (E) and myeloid progenitor subsets (CMP, GMP, MEP) (F) in the BM (per hindlimb) of mice in (D).
(G) Flow cytometric analyses of the BM from WT and *Mlkl*$^{-/-}$ mice in (D). Numbers indicate percentage (±SEM). Data represent four mice per genotype (D–G).
(H) Colony count of sorted FLT3-ITD-transduced WT, *Ripk3*$^{-/-}$, and *Mlkl*$^{-/-}$ ST-HSC.
(I) Flow cytometric analysis of in vitro cultures of FLT3-ITD-transduced WT and *Mlkl*$^{-/-}$ sorted ST-HSC or CMP. Numbers in plots indicate percentage. Data represent one experiment with 12 mice per genotype (H–I).
Error bars represent means ± SEM. p Values Student's t test: *p < 0.05, **p < 0.005, ***p < 0.0005. See also Figure S4.

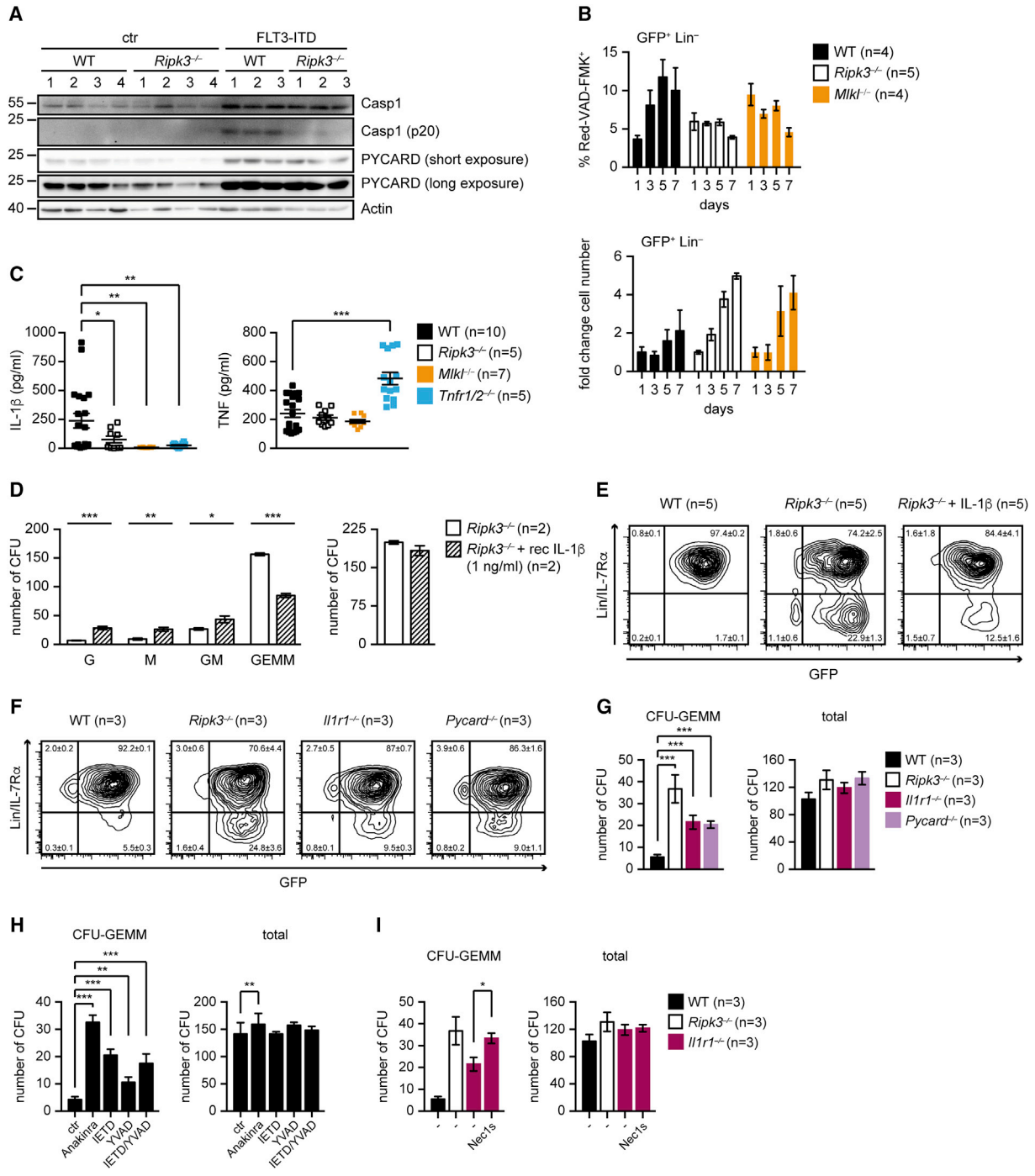

Figure 5. RIPK3 Controls Inflammasome Activation in Malignant Progenitors

(A) Immunoblots of three to four samples each of 5-FU-enriched HSPC (ctr) or FLT3-ITD-transduced WT and *Ripk3*$^{-/-}$ BM cultured for 7 days. Data are representative of three independent experiments.

(B) Red-VAD-FMK staining and fold change of GFP^{+} Lin^{-} FLT3-ITD-transduced WT, *Ripk3*$^{-/-}$, and *Mlkl*$^{-/-}$ BM cells over time. Data represent one experiment.

(C) Secreted IL-1β and TNF from CFU assays of FLT3-ITD-transduced WT, *Ripk3*$^{-/-}$, *Mlkl*$^{-/-}$, and *Tnfr1/2*$^{-/-}$ BM. Data represent two independent experiments.

(D) Colony count of FLT3-ITD-transduced *Ripk3*$^{-/-}$ BM cultured in the presence or absence of recombinant mouse IL-1β (1 ng/ml). Data are representative of three independent experiments.

(E) Flow cytometric analysis of FLT3-ITD-transduced WT and *Ripk3*$^{-/-}$ BM cultured in the presence or absence of recombinant mouse IL-1β (1 ng/ml). Numbers in plots indicate percentage (±SEM). Data are representative of two independent experiments.

(F) Flow cytometric analysis of cultures of FLT3-ITD-transduced WT, *Ripk3*$^{-/-}$, *Il1r1*$^{-/-}$, and *Pycard*$^{-/-}$ BM. Numbers in plots indicate percentage (±SEM). Data are representative of two independent experiments.

(legend continued on next page)

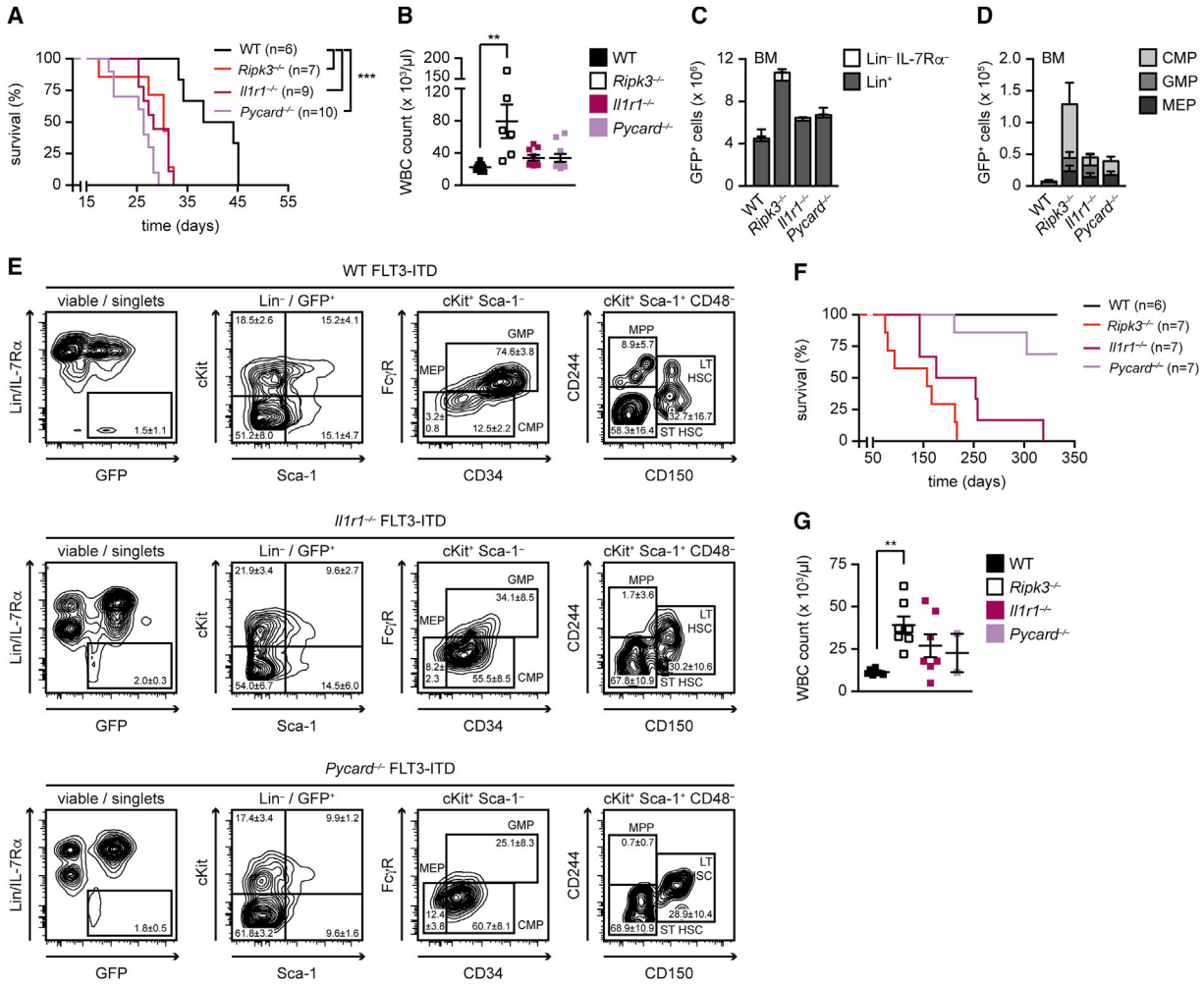

Figure 6. PYCARD- and IL-1R-Dependent Signaling Suppress FLT3-ITD Leukemogenesis

(A) Survival of mice transplanted with FLT3-ITD-transduced WT, *Ripk3*$^{-/-}$, *Il1r1*$^{-/-}$, or *Pycard*$^{-/-}$ BM. Median survival WT 41 days versus 30, 28, and 26 days for *Ripk3*$^{-/-}$, *Il1r1*$^{-/-}$, and *Pycard*$^{-/-}$, respectively.

(B) Peripheral WBC counts of mice in (A).

(C and D) Absolute numbers of GFP^{+} mature (Lin^{+}) and HSPC (Lin^{-}IL-7Rα^{-}) (C) and myeloid progenitor subsets (CMP, GMP, MEP) (D) in the BM (per hindlimb) of WT, *Ripk3*$^{-/-}$, *Il1r1*$^{-/-}$, and *Pycard*$^{-/-}$ mice in (A).

(E) Flow cytometric analysis of WT, *Il1r1*$^{-/-}$, and *Pycard*$^{-/-}$ mice in (A). Numbers indicate percentage (±SEM).

(F) Survival of mice serially transplanted with GFP^{+} splenocytes from primary FLT3-ITD-transplanted WT, *Ripk3*$^{-/-}$, *Il1r1*$^{-/-}$, or *Pycard*$^{-/-}$ mice. Median survival WT 128 days versus *Il1r1*$^{-/-}$ 201 days. Data are representative of one experiment.

(G) Peripheral WBC counts of mice in (F).

Each dot represents a mouse, and error bars represent means ± SEM. p Values (A) and (F) Mantel-Cox test, otherwise Student's t test: **p < 0.005, ***p < 0.0005. See also Figure S6.

However, the numbers of these progenitors were increased in *Ripk3*$^{-/-}$ with significantly elevated ST-HSC also arising from *Ripk3*$^{-/-}$ (Figure 8E). These data support the notion that RIPK3 suppresses AML-ETO leukemogenesis by restricting the survival of progenitor cells.

In contrast, in MLL-translocated AML, *RIPK3* expression is not reduced (Figure 8G), and, as expected, *Ripk3* deletion did not affect MLL-ENL-driven leukemogenesis in experimental mice (Figure 8H). The leukemic onset, WBC counts, and leukemic burden remained unaffected by the genetic loss of *Ripk3*

(G) Colony count of FLT3-ITD-transduced WT, *Ripk3*$^{-/-}$, *Il1r1*$^{-/-}$, and *Pycard*$^{-/-}$ BM. Data are representative of two independent experiments.

(H) Colony count of FLT3-ITD-transduced WT BM in the presence of anakinra, IETD, and/or YVAD. Data depict five mice and are representative of two independent experiments.

(I) Colony count of FLT3-ITD-transduced WT, *Ripk3*$^{-/-}$, and *Il1r1*$^{-/-}$ BM in the presence or absence of Nec1s. Data are representative of two independent experiments.

Each dot represents a mouse, and error bars represent means ± SEM. p Values Student's t test: *p < 0.05, **p < 0.005, ***p < 0.0005. See also Figure S5.

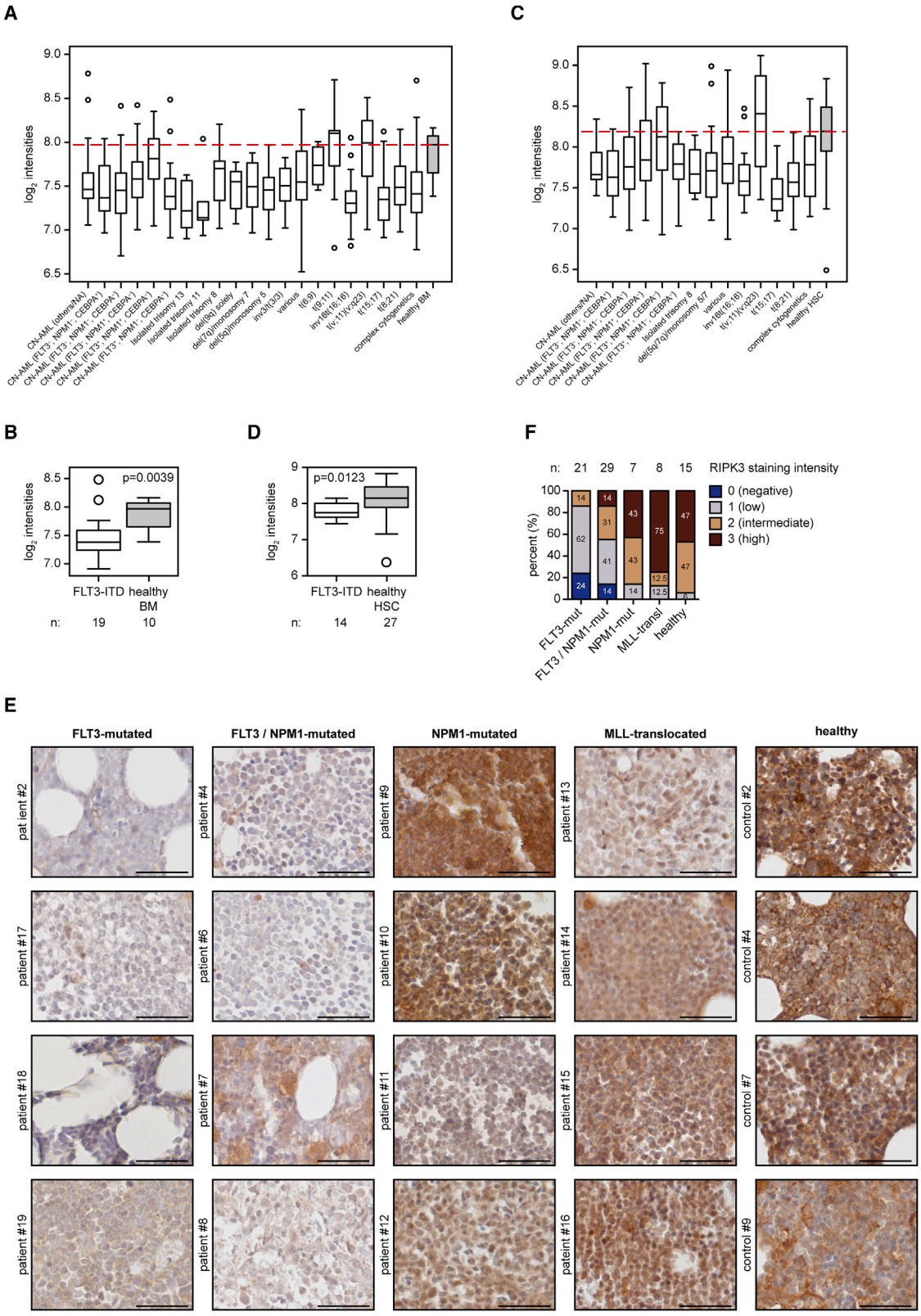

Figure 7. Expression of *RIPK3* Is Reduced in Human FLT3-Mutated AML

(A and B) Gene expression profiles (GEP) for *RIPK3* obtained from 562 de novo AML patient samples and ten healthy BM controls (GEO: GSE37642).

(C and D) GEP for *RIPK3* obtained from 461 de novo AML patient samples and 27 healthy HSC controls (GEO: GSE6891). AML subtypes are defined by standardized cytogenetic or molecular genetic aberrations. Mean expression of *RIPK3* in healthy controls is indicated by the red dashed line. Data in (A–D) are

(legend continued on next page)

(Figures 8H, 8I, and S8E–S8H). No significant differences between mice transplanted with WT or *Ripk3*$^{-/-}$MLL-ENL were observed within the HSPC compartment (Figures 8J–8L and S8I). These data are in line with the human gene expression data that suggested leukemogenesis driven by MLL translocations was independent of RIPK3 activity.

These data identify RIPK3-dependent cell death and cellular differentiation as tumor-suppressive mechanisms for several AML subtypes as suppression of *RIPK3* granted LIC a clear survival advantage. Thus, the re-activation of RIPK3-dependent signaling might help to combat AML clinically in specific AML subtypes.

DISCUSSION

We demonstrate here that RIPK3 signaling is a key tumor-suppressive mechanism in AML and identify the critical function of inflammatory cell death not only for LIC survival but also for differentiation in AML. The ability to evade programmed cell death is a common feature of cancer cells, however efforts are currently focused on re-activating apoptotic forms of cell death in AML (Jilg et al., 2016; Vo et al., 2012).

In human patients, FLT3 mutations occur late in leukemogenesis and modulate existing pre-leukemic clones that already carry mutations in epigenetic modifiers or transcription factors (Welch et al., 2012). Our analysis of human expression data showed that the RIPK3/MLKL pathway is suppressed in several AML subgroups. This suggests that selection for RIPK3-deficient clones exists and is likely a common feature of LIC in several AML subtypes.

The mechanism for the reduced *RIPK3* and *MLKL* expression remains unclear. Database searches of 150 AML exomes and 50 AML genomes taken from the human cancer gene atlas (TCGA) and an alternative cohort of 24 AML exomes did not show relevant numbers of somatic mutations of *RIPK3* in de novo AML (Cancer Genome Atlas Research Network, 2013; Welch et al., 2012). However, expression levels might be regulated by several molecular mechanisms including DNA methylation, microRNA, or transcription factors. These mechanisms have already been implicated in modulating *IL1B* expression in human AML samples, particularly in the CD34^{+}/CD38^{-} compartment, and are in line with our data that showed dampening of IL-1R signaling was central for myeloid leukemogenesis (Marcucci et al., 2008; Su et al., 2015; Yang et al., 2013). In addition, our findings now add a post-transcriptional layer of control on IL-1β signaling mediated by RIPK3-dependent activation of the inflammasome. It has been clearly established that both the necroptosis and inflammasome pathways are heavily regulated by post-translational modifications such as phosphorylation (Cho et al., 2009) and ubiquitylation (Onizawa et al., 2015; Yabal et al., 2014). This is illustrated by our finding of reduced proteolysis of caspase-1 in *Ripk3*$^{-/-}$ precursor cells, which is in line with the previously reported post-translational regulation of the inflammasome by RIPK3 in mature myeloid cells (Lawlor et al., 2015; Yabal et al., 2014). This argues that pharmacological re-activation of RIPK3 signaling might serve as a therapeutic approach to induce resistant LIC to undergo cell death.

Cell-death induction downstream of RIPK3 limits leukemia development, however the relative contributions of necroptotic or apoptotic signaling remain unclear. Our data, showing the partly MLKL-independent caspase activation and cell-death induction, as well as low MLKL protein expression in leukemic cells, suggest that an apoptotic component might contribute to the death of LIC (Lawlor et al., 2015; Mandal et al., 2014; Yabal et al., 2014). The aggravated phenotype of *Mlkl*$^{-/-}$ leukemia potentially originates also from failed inflammasome formation (Kang et al., 2015).

Irrespective of additional pre-existing mutations, FLT3-ITD induces aberrant gene expression and methylation patterns that activate pathways associated with immune response and cellular stress (Cauchy et al., 2015). This inflammatory program instructs leukemic cells to produce cytokines, such as TNF and IL-1β, in order to promote survival. In AML, TNF has been clearly shown to promote the proliferation and survival of leukemic cells (Volk et al., 2014). This is remarkable, because TNFR signaling plays an opposing role in healthy HSPC, where it serves as a potent repressor of HSPC self-renewal (Pronk et al., 2011). This illustrates that a dichotomy between pro-survival and death-inducing functions of TNFR signaling exists in leukemic cells. Our data provide one molecular mechanism that protects leukemic cells against TNFR-dependent cell death by positive selection for cells that repress RIPK3 activation and subsequent cell death.

In addition to IL-1β, necroptotically dying cells release a plethora of DAMP and other cytokines, which together instruct a pro-inflammatory environment that likely promotes differentiation. This argues that exogenous activation of necroptosis might serve as a therapeutic principle to induce LIC cell death and differentiation in AML. The paradigm for using differentiation-inducing therapy in AML is exemplified by the efficacy of all-*trans* retinoic acid (ATRA) in treating acute promyelocytic leukemia (APL) (Schenk et al., 2012).

In summary, our findings provide evidence for a tumor-suppressive function of RIPK3-mediated signaling in AML. RIPK3-driven cell death and inflammasome-mediated IL-1β release restrict myeloid leukemogenesis by killing transformed progenitor cells and by enhancing differentiation of LICs.

depicted as Tukey boxplots, depicting the median, the upper and lower quartiles, and whiskers with maximum 1.5 interquartile range. Outliers are plotted as individual points.

(E) Representative images of immunohistochemistry of BM biopsies from AML patients of indicated AML subtypes and healthy controls stained for RIPK3 (brown) and counterstained with hematoxylin (blue). RIPK3-specific staining was localized to the cytoplasm. Infiltration rates as follows: #12, 40%; #7, #10, and #14, 50%; all others between 75% and >90%. Scale bar is 50 μm.

(F) Quantification of RIPK3 staining intensity in (E). Quantification was performed blinded. Cytoplasmatic RIPK3 staining intensity in AML blasts was semi-quantitatively assessed and classified as negative, low, intermediate, or high. RIPK3 staining intensity was significantly different between AML subtypes.

p Values (B) and (D) Student's t test; p values (F) Pearson's chi-squared test: $p < 0.0001$. See also Figure S7.

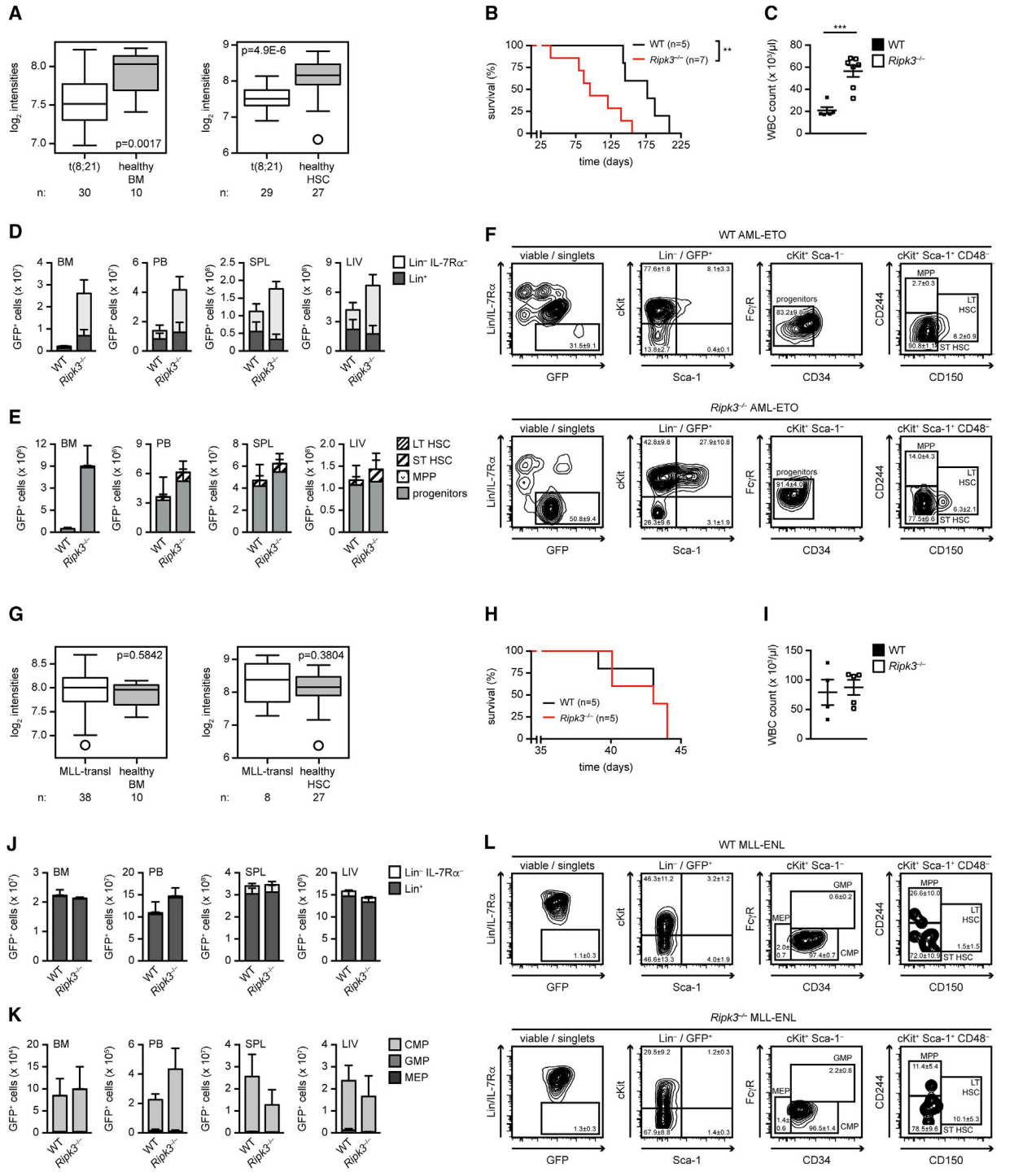

Figure 8. Suppression of RIPK3 Accelerates Leukemogenesis Driven by t(8;21) but Not MLL Translocations

(A) Gene expression profiles for *RIPK3* in AML-ETO (t(8;21))-translocated AML samples, from GEO: GSE37642 (left) and GEO: GSE6891 (right), respectively.

(B) Survival of mice transplanted with AML1-ETO9a-transduced WT or *Ripk3*$^{-/-}$ BM. Median survival WT 176 days versus 93 days for *Ripk3*$^{-/-}$. Data are representative of two independent experiments.

(C) Peripheral WBC counts of mice in (B).

(D and E) Absolute numbers of GFP^{+} mature (Lin^{+}) and HSPC (Lin^{-}IL-7Rα^{-}) (D) and myeloid progenitors (E) in the BM (per hindlimb), PB, SPL, and LIV of WT and *Ripk3*$^{-/-}$ mice in (B).

(F) Flow cytometric analysis of WT and *Ripk3*$^{-/-}$ mice in (B). Numbers indicate percentage (±SEM).

(legend continued on next page)

EXPERIMENTAL PROCEDURES

Mice

Ripk3$^{-/-}$ mice were obtained under a material transfer agreement from Genentech and have been previously described (Newton et al., 2004). *Il1r1* ^{tm1Imx}*/J* (*Il1r1*$^{-/-}$) (Glaccum et al., 1997) mice were purchased from Jackson Laboratories. *Tnfrsf1a* ^{tm1Imx} *Tnfrsf1b* $^{tm1Imx/J}$ (*Tnfr1/2*$^{-/-}$), *Pycard*$^{-/-}$, and *Mlkl*$^{-/-}$ mice have been previously described (Mariathasan et al., 2004; Murphy et al., 2013; Peschon et al., 1998). Animals were maintained under specific pathogen-free conditions, and all animal experiments were approved by the District Government of Upper Bavaria.

In Vitro Progenitor Cell Analysis

For flow cytometry and mRNA expression analysis, FLT3-ITD-transduced BM cells were cultured in RPMI/10% fetal calf serum for 7 days in the absence of cytokines. For CFU assays, cultures were performed in murine methylcellulose medium (Methocult, STEMCELL Technologies). Colonies were counted after 10 days.

For analysis of CFU cell viability, colonies were grown for 10 days in the presence of PI and representative CFU GEMM were imaged. Cytokines were quantified using cytometric bead array (BD Biosciences).

Human Primary AML Samples

Primary AML samples were obtained from patients enrolled in the clinical trial AMLCG-2008 (http://clinicaltrial.gov identifier NCT01382147), the AML register protocol of the AML Register and Biomaterial Database of the German Leukemia Study Alliance, the AML register protocol of the German AML Cooperative Group Version 2.0 from January 6, 2011, the AML register protocol of the German AML study group, or treated at the III. Medical Department at the Technical University of Munich after approval of the local ethics committee (approval no. 62/16 S from February 10, 2016 to 2790/10 from April 30, 2010). Informed consent was obtained from patients at study entry. Immunohistochemistry and gene expression analyses were performed as described in Supplemental Information.

Statistical Analyses

For statistical analyses, p values were determined by applying the two-tailed t test for independent samples. Survival curves were analyzed using the Mantel-Cox test. The histologic samples were analyzed using the Pearson chi-squared test. All values are expressed as means ± SEM, and *$p < 0.05$, **$p < 0.005$, and ***$p < 0.0005$ were performed with GraphPad Prism software or SPSS. If not otherwise indicated experiments represent at least eight mice per genotype.

ACCESSION NUMBERS

The accession number for the microarray datasets reported in this paper is GEO: GSE79040.

SUPPLEMENTAL INFORMATION

Supplemental Information includes Supplemental Experimental Procedures and eight figures and can be found with this article online at http://dx.doi.org/10.1016/j.ccell.2016.06.002.

AUTHOR CONTRIBUTIONS

Conceptualization, P.J.J., O.G., M.H., U.H., M.Y.; Methodology, U.H., J.S.H.; Investigation, U.H., M.Y., J.S.H., T.E., R.R., E.M., S.R.; Formal Analysis, T.E., R.R., J.S.H.; Resources, S.J., J.K., G.M., F.R., H.K., K.S., W.W., C.P., J.R., M.H., K.S., O.G.; Data Curation, T.H., K.S.; Writing – Original Draft/Review & Editing, P.J.J., U.H., M.Y.; Supervision, P.J.J.; Funding Acquisition, P.J.J., M.Y.

ACKNOWLEDGMENTS

We thank P. Cockerill and C. Bonifer for sharing of data and critical discussion; Genentech, J. Murphy, A. Linkermann, U. Maurer, W.-W. Lynn Wong for mice; M. Schmidt-Supprian, R. Oostendorp for critical discussion; the Microarray Unit of the Genomics & Proteomics Core Facility at the DKFZ for providing excellent gene expression profiling services. Grant support by a Max Eder-Program grant from the Deutsche Krebshilfe (program #111738), an HFSP grant (program #RGY0073/2012), a Deutsche Jose Carreras Leukämie Stiftung (DJCLS R 12/22), DFG (FOR2036) to P.J.J.; Else Kröner-Fresenius-Stiftung grant 2014_A185 to P.J.J. and M.Y.; ERC Starting Grant and Bavarian Molecular Biosystems Research_Network to O.G.; DFG SFB 1243/A07 to K.S. Deutsche Krebshilfe grant no. 1097154, Teilprojekt A,D to H.K.; Hans-und-Klementia-Langmatz Stiftung grant to S.J.; ERC Starting grant (LiverCancerMechanism), an SFB TR36 initiative, the Stiftung für Biomedizinische Forschung (Hofschneider Foundation), and the Helmholtz Alliance Pre-clinical Cancer Center (PCCC) to M.H.

Received: September 29, 2015
Revised: March 4, 2016
Accepted: June 1, 2016
Published: July 11, 2016

REFERENCES

Bertrand, M.J., Milutinovic, S., Dickson, K.M., Ho, W.C., Boudreault, A., Durkin, J., Gillard, J.W., Jaquith, J.B., Morris, S.J., and Barker, P.A. (2008). cIAP1 and cIAP2 facilitate cancer cell survival by functioning as E3 ligases that promote RIP1 ubiquitination. Mol. Cell *30*, 689–700.

Cai, Z., Jitkaew, S., Zhao, J., Chiang, H.C., Choksi, S., Liu, J., Ward, Y., Wu, L.G., and Liu, Z.G. (2014). Plasma membrane translocation of trimerized MLKL protein is required for TNF-induced necroptosis. Nat. Cell Biol. *16*, 55–65.

Cancer Genome Atlas Research Network. (2013). Genomic and epigenomic landscapes of adult de novo acute myeloid leukemia. N. Engl. J. Med. *368*, 2059–2074.

Cauchy, P., James, S.R., Zacarias-Cabeza, J., Ptasinska, A., Imperato, M.R., Assi, S.A., Piper, J., Canestraro, M., Hoogenkamp, M., Raghavan, M., et al. (2015). Chronic FLT3-ITD signaling in acute myeloid leukemia is connected to a specific chromatin signature. Cell Rep. *12*, 821–836.

Cho, Y., Challa, S., Moquin, D., Genga, R., Ray, T.D., Guildford, M., and Chan, F.K.-M. (2009). Phosphorylation-driven assembly of the RIP1-RIP3 complex regulates programmed necrosis and virus-induced inflammation. Cell *137*, 1112–1123.

(G) Gene expression profiles for *RIPK3* in MLL-translocated (MLL-transl) AML samples, from GEO: GSE37642 (left) and GEO: GSE6891 (right), respectively. Data in (A) and (G) are depicted as Tukey boxplots, depicting the median, the upper and lower quartiles, and whiskers with maximum 1.5 interquartile range. Outliers are plotted as individual points.

(H) Survival of WT mice transplanted with MLL-ENL-transduced WT or *Ripk3*$^{-/-}$ BM. Median survival WT 43 days versus *Ripk3*$^{-/-}$ 43 days. Data are representative of two independent experiments.

(I) Peripheral WBC counts of mice in (H).

(J and K) Absolute numbers of GFP$^+$ mature (Lin$^+$) and HSPC (Lin$^-$IL-7Rα^-) (J) and myeloid progenitor subsets (CMP, GMP, MEP) (K) in the BM (per hindlimb), PB, SPL, and LIV of WT and *Ripk3*$^{-/-}$ mice in (H).

(L) Flow cytometric analysis of WT and *Ripk3*$^{-/-}$ mice in (H). Numbers indicate percentage (±SEM).

Each dot represents a mouse, and error bars represent means ± SEM. p Values (B) and (H) Mantel-Cox test, otherwise Student's t test: **$p < 0.005$, ***$p < 0.0005$. See also Figure S8.

Chu, S.H., Heiser, D., Li, L., Kaplan, I., Collector, M., Huso, D., Sharkis, S.J., Civin, C., and Small, D. (2012). FLT3-ITD knockin impairs hematopoietic stem cell quiescence/homeostasis, leading to myeloproliferative neoplasm. Cell Stem Cell *11*, 346–358.

Duprez, L., Takahashi, N., Van Hauwermeiren, F., Vandendriessche, B., Goossens, V., Vanden Berghe, T., Declercq, W., Libert, C., Cauwels, A., and Vandenabeele, P. (2011). RIP kinase-dependent necrosis drives lethal systemic inflammatory response syndrome. Immunity *35*, 908–918.

Glaccum, M.B., Stocking, K.L., Charrier, K., Smith, J.L., Willis, C.R., Maliszewski, C., Livingston, D.J., Peschon, J.J., and Morrissey, P.J. (1997). Phenotypic and functional characterization of mice that lack the type I receptor for IL-1. J. Immunol. *159*, 3364–3371.

Herold, T., Metzeler, K.H., Vosberg, S., Hartmann, L., Rollig, C., Stolzel, F., Schneider, S., Hubmann, M., Zellmeier, E., Ksienzyk, B., et al. (2014). Isolated trisomy 13 defines a homogeneous AML subgroup with high frequency of mutations in spliceosome genes and poor prognosis. Blood *124*, 1304–1311.

Huntly, B.J., and Gilliland, D.G. (2005). Leukaemia stem cells and the evolution of cancer-stem-cell research. Nat. Rev. Cancer *5*, 311–321.

Jacobsen, S.E., Ruscetti, F.W., Okkenhaug, C., Lien, E., Ortiz, M., Veiby, O.P., and Keller, J.R. (1994). Distinct and direct synergistic effects of IL-1 and IL-6 on proliferation and differentiation of primitive murine hematopoietic progenitor cells in vitro. Exp. Hematol. *22*, 1064–1069.

Jilg, S., Reidel, V., Muller-Thomas, C., Konig, J., Schauwecker, J., Hockendorf, U., Huberle, C., Gorka, O., Schmidt, B., Burgkart, R., et al. (2016). Blockade of BCL-2 proteins efficiently induces apoptosis in progenitor cells of high-risk myelodysplastic syndromes patients. Leukemia *30*, 112–123.

Kang, S., Fernandes-Alnemri, T., Rogers, C., Mayes, L., Wang, Y., Dillon, C., Roback, L., Kaiser, W., Oberst, A., Sagara, J., et al. (2015). Caspase-8 scaffolding function and MLKL regulate NLRP3 inflammasome activation downstream of TLR3. Nat. Commun. *6*, 7515.

Kelly, L.M., Liu, Q., Kutok, J.L., Williams, I.R., Boulton, C.L., and Gilliland, D.G. (2002). FLT3 internal tandem duplication mutations associated with human acute myeloid leukemias induce myeloproliferative disease in a murine bone marrow transplant model. Blood *99*, 310–318.

Lawlor, K.E., Khan, N., Mildenhall, A., Gerlic, M., Croker, B.A., D'Cruz, A.A., Hall, C., Kaur Spall, S., Anderton, H., Masters, S.L., et al. (2015). RIPK3 promotes cell death and NLRP3 inflammasome activation in the absence of MLKL. Nat. Commun. *6*, 6282.

Mandal, P., Berger, S.B., Pillay, S., Moriwaki, K., Huang, C., Guo, H., Lich, J.D., Finger, J., Kasparcova, V., Votta, B., et al. (2014). RIP3 induces apoptosis independent of pronecrotic kinase activity. Mol. Cell *56*, 481–495.

Marcucci, G., Radmacher, M.D., Maharry, K., Mrózek, K., Ruppert, A.S., Paschka, P., Vukosavljevic, T., Whitman, S.P., Baldus, C.D., Langer, C., et al. (2008). MicroRNA expression in cytogenetically normal acute myeloid leukemia. N. Engl. J. Med. *358*, 1919–1928.

Mariathasan, S., Newton, K., Monack, D.M., Vucic, D., French, D.M., Lee, W.P., Roose-Girma, M., Erickson, S., and Dixit, V.M. (2004). Differential activation of the inflammasome by caspase-1 adaptors ASC and Ipaf. Nature *430*, 213–218.

Mead, A.J., Kharazi, S., Atkinson, D., Macaulay, I., Pecquet, C., Loughran, S., Lutteropp, M., Woll, P., Chowdhury, O., Luc, S., et al. (2013). FLT3-ITDs instruct a myeloid differentiation and transformation bias in lymphomyeloid multipotent progenitors. Cell Rep. *3*, 1766–1776.

Murphy, J.M., Czabotar, P.E., Hildebrand, J.M., Lucet, I.S., Zhang, J.G., Alvarez-Diaz, S., Lewis, R., Lalaoui, N., Metcalf, D., Webb, A.I., et al. (2013). The pseudokinase MLKL mediates necroptosis via a molecular switch mechanism. Immunity *39*, 443–453.

Newton, K., Sun, X., and Dixit, V.M. (2004). Kinase RIP3 is dispensable for normal NF- Bs, signaling by the B-cell and T-cell receptors, tumor necrosis factor receptor 1, and toll-like receptors 2 and 4. Mol. Cell Biol. *24*, 1464–1469.

Nugues, A.L., El Bouazzati, H., Hetuin, D., Berthon, C., Loyens, A., Bertrand, E., Jouy, N., Idziorek, T., and Quesnel, B. (2014). RIP3 is downregulated in human myeloid leukemia cells and modulates apoptosis and caspase-mediated p65/RelA cleavage. Cell Death Dis. *5*, e1384.

Onizawa, M., Oshima, S., Schulze-Topphoff, U., Oses-Prieto, J.A., Lu, T., Tavares, R., Prodhomme, T., Duong, B., Whang, M.I., Advincula, R., et al. (2015). The ubiquitin-modifying enzyme A20 restricts ubiquitination of the kinase RIPK3 and protects cells from necroptosis. Nat. Immunol. *16*, 618–627.

Pasparakis, M., and Vandenabeele, P. (2015). Necroptosis and its role in inflammation. Nature *517*, 311–320.

Peschon, J.J., Torrance, D.S., Stocking, K.L., Glaccum, M.B., Otten, C., Willis, C.R., Charrier, K., Morrissey, P.J., Ware, C.B., and Mohler, K.M. (1998). TNF receptor-deficient mice reveal divergent roles for p55 and p75 in several models of inflammation. J. Immunol. *160*, 943–952.

Pronk, C.J., Veiby, O.P., Bryder, D., and Jacobsen, S.E. (2011). Tumor necrosis factor restricts hematopoietic stem cell activity in mice: involvement of two distinct receptors. J. Exp. Med. *208*, 1563–1570.

Rickard, J.A., O'Donnell, J.A., Evans, J.M., Lalaoui, N., Poh, A.R., Rogers, T., Vince, J.E., Lawlor, K.E., Ninnis, R.L., Anderton, H., et al. (2014). RIPK1 regulates RIPK3-MLKL-driven systemic inflammation and emergency hematopoiesis. Cell *157*, 1175–1188.

Schenk, T., Chen, W.C., Gollner, S., Howell, L., Jin, L., Hebestreit, K., Klein, H.U., Popescu, A.C., Burnett, A., Mills, K., et al. (2012). Inhibition of the LSD1 (KDM1A) demethylase reactivates the all-trans-retinoic acid differentiation pathway in acute myeloid leukemia. Nat. Med. *18*, 605–611.

Schroder, K., and Tschopp, J. (2010). The inflammasomes. Cell *140*, 821–832.

Shlush, L.I., Zandi, S., Mitchell, A., Chen, W.C., Brandwein, J.M., Gupta, V., Kennedy, J.A., Schimmer, A.D., Schuh, A.C., Yee, K.W., et al. (2014). Identification of pre-leukaemic haematopoietic stem cells in acute leukaemia. Nature *506*, 328–333.

Su, R., Lin, H.S., Zhang, X.H., Yin, X.L., Ning, H.M., Liu, B., Zhai, P.F., Gong, J.N., Shen, C., Song, L., et al. (2015). MiR-181 family: regulators of myeloid differentiation and acute myeloid leukemia as well as potential therapeutic targets. Oncogene *34*, 3226–3239.

Takizawa, H., Boettcher, S., and Manz, M.G. (2012). Demand-adapted regulation of early hematopoiesis in infection and inflammation. Blood *119*, 2991–3002.

Tenen, D.G. (2003). Disruption of differentiation in human cancer: AML shows the way. Nat. Rev. Cancer *3*, 89–101.

Vassiliou, G.S., Cooper, J.L., Rad, R., Li, J., Rice, S., Uren, A., Rad, L., Ellis, P., Andrews, R., Banerjee, R., et al. (2011). Mutant nucleophosmin and cooperating pathways drive leukemia initiation and progression in mice. Nat. Genet. *43*, 470–475.

Verhaak, R.G., Wouters, B.J., Erpelinck, C.A., Abbas, S., Beverloo, H.B., Lugthart, S., Lowenberg, B., Delwel, R., and Valk, P.J. (2009). Prediction of molecular subtypes in acute myeloid leukemia based on gene expression profiling. Haematologica *94*, 131–134.

Vo, T.T., Ryan, J., Carrasco, R., Neuberg, D., Rossi, D.J., Stone, R.M., Deangelo, D.J., Frattini, M.G., and Letai, A. (2012). Relative mitochondrial priming of myeloblasts and normal HSCs determines chemotherapeutic success in AML. Cell *151*, 344–355.

Volk, A., Li, J., Xin, J., You, D., Zhang, J., Liu, X., Xiao, Y., Breslin, P., Li, Z., Wei, W., et al. (2014). Co-inhibition of NF-kappaB and JNK is synergistic in TNF-expressing human AML. J. Exp. Med. *211*, 1093–1108.

Wang, H., Sun, L., Su, L., Rizo, J., Liu, L., Wang, L.F., Wang, F.S., and Wang, X. (2014). Mixed lineage kinase domain-like protein MLKL causes necrotic membrane disruption upon phosphorylation by RIP3. Mol. Cell *54*, 133–146.

Welch, J.S., Ley, T.J., Link, D.C., Miller, C.A., Larson, D.E., Koboldt, D.C., Wartman, L.D., Lamprecht, T.L., Liu, F., Xia, J., et al. (2012). The origin and evolution of mutations in acute myeloid leukemia. Cell *150*, 264–278.

Wong, W.W., Vince, J.E., Lalaoui, N., Lawlor, K.E., Chau, D., Bankovacki, A., Anderton, H., Metcalf, D., O'Reilly, L., Jost, P.J., et al. (2014). cIAPs and XIAP regulate myelopoiesis through cytokine production in an RIPK1- and RIPK3-dependent manner. Blood *123*, 2562–2572.

Yabal, M., Muller, N., Adler, H., Knies, N., Gross, C.J., Damgaard, R.B., Kanegane, H., Ringelhan, M., Kaufmann, T., Heikenwalder, M., et al. (2014). XIAP restricts TNF- and RIP3-dependent cell death and inflammasome activation. Cell Rep. *7*, 1796–1808.

Yan, M., Kanbe, E., Peterson, L.F., Boyapati, A., Miao, Y., Wang, Y., Chen, I.M., Chen, Z., Rowley, J.D., Willman, C.L., and Zhang, D.E. (2006). A previously unidentified alternatively spliced isoform of t(8;21) transcript promotes leukemogenesis. Nat. Med. *12*, 945–949.

Yang, J., Ikezoe, T., Nishioka, C., Nobumoto, A., and Yokoyama, A. (2013). IL-1beta inhibits self-renewal capacity of dormant CD34(+)/CD38(-) acute myelogenous leukemia cells in vitro and in vivo. Int. J. Cancer *133*, 1967–1981.

Zhao, J.L., Ma, C., O'Connell, R.M., Mehta, A., DiLoreto, R., Heath, J.R., and Baltimore, D. (2014). Conversion of danger signals into cytokine signals by hematopoietic stem and progenitor cells for regulation of stress-induced hematopoiesis. Cell Stem Cell *14*, 445–459.

Cancer Cell, Volume *30*

Supplemental Information

RIPK3 Restricts Myeloid Leukemogenesis by Promoting Cell Death and Differentiation of Leukemia Initiating Cells

Ulrike Höckendorf, Monica Yabal, Tobias Herold, Enkhtsetseg Munkhbaatar, Stephanie Rott, Stefanie Jilg, Johanna Kauschinger, Giovanni Magnani, Florian Reisinger, Michael Heuser, Hans Kreipe, Karl Sotlar, Thomas Engleitner, Roland Rad, Wilko Weichert, Christian Peschel, Jürgen Ruland, Mathias Heikenwalder, Karsten Spiekermann, Julia Slotta-Huspenina, Olaf Groß, and Philipp J. Jost

Supplemental Data

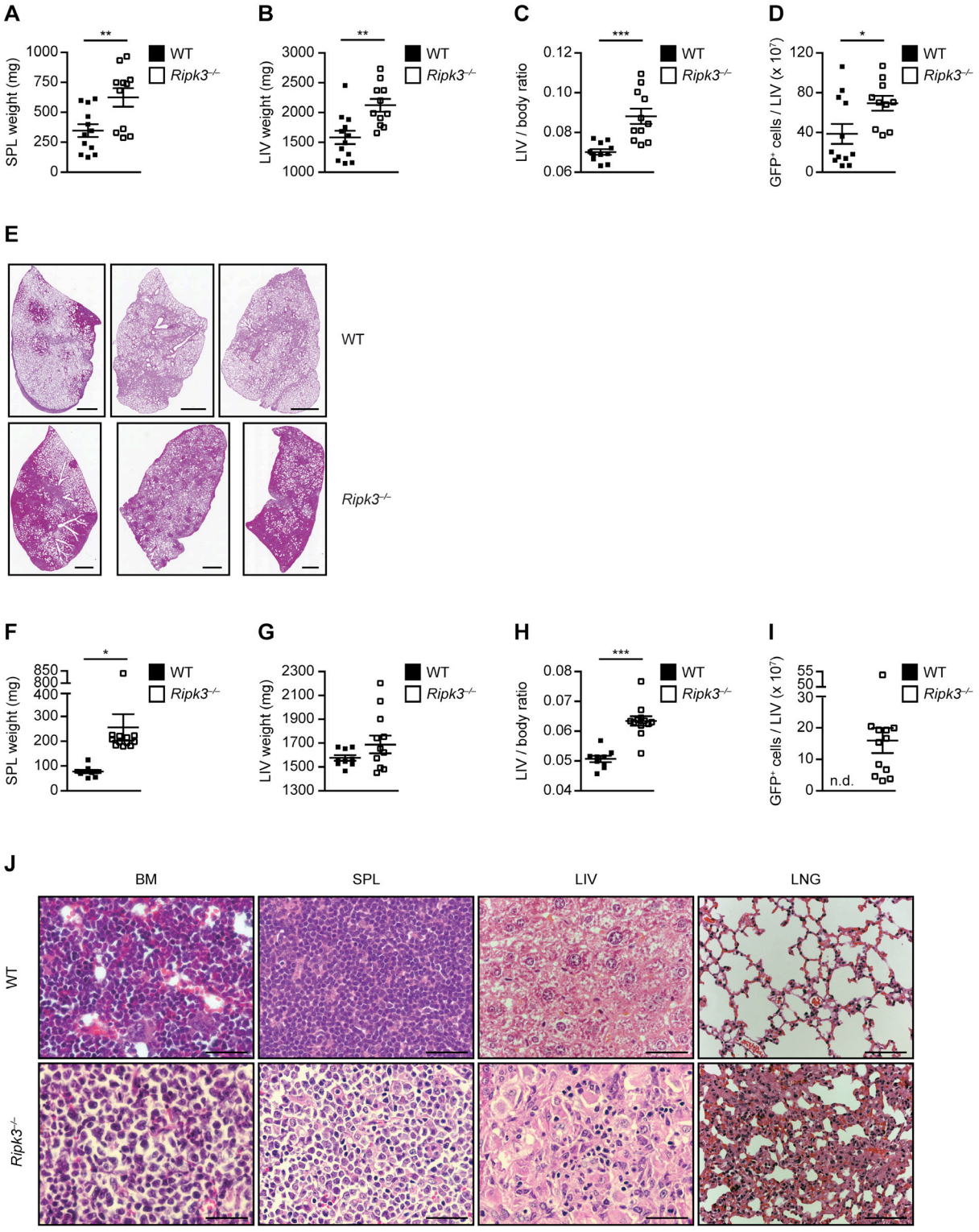

Figure S1. Increased leukemic burden in *Ripk3*$^{-/-}$ FLT3-ITD mice. Related to Figure 1.
(A) SPL and (B) LIV weight of mice in (Figure 1A) transplanted with FLT3-ITD–transduced WT and *Ripk3*$^{-/-}$ BM. (C) LIV/body ratio and (D) absolute numbers of GFP^{+} cells/LIV from mice in (Figure 1A). Data in (A-D) depict 12 WT and 11 *Ripk3*$^{-/-}$ mice. (E) H&E of the lung collected from mice in (Figure 1A). Scale bar is 500 µm. (F) SPL and (G) LIV weight of mice in (Figure 1H) serially transplanted with GFP^{+} splenocytes from primary FLT3-ITD–transplanted WT and *Ripk3*$^{-/-}$ mice. (H) LIV/body ratio and (I) absolute numbers of GFP^{+} cells/LIV from mice in (Figure 1H). Data in (F-I) depict nine WT and 12 *Ripk3*$^{-/-}$ mice. (J) H&E of BM, SPL, LIV and LNG collected from mice in (Figure 1H). Scale bar is 40 µm. Each dot represents a mouse and error bars represent mean ± SEM. p values Student´s t test *p<0.05, **p<0.005, ***p<0.0005.

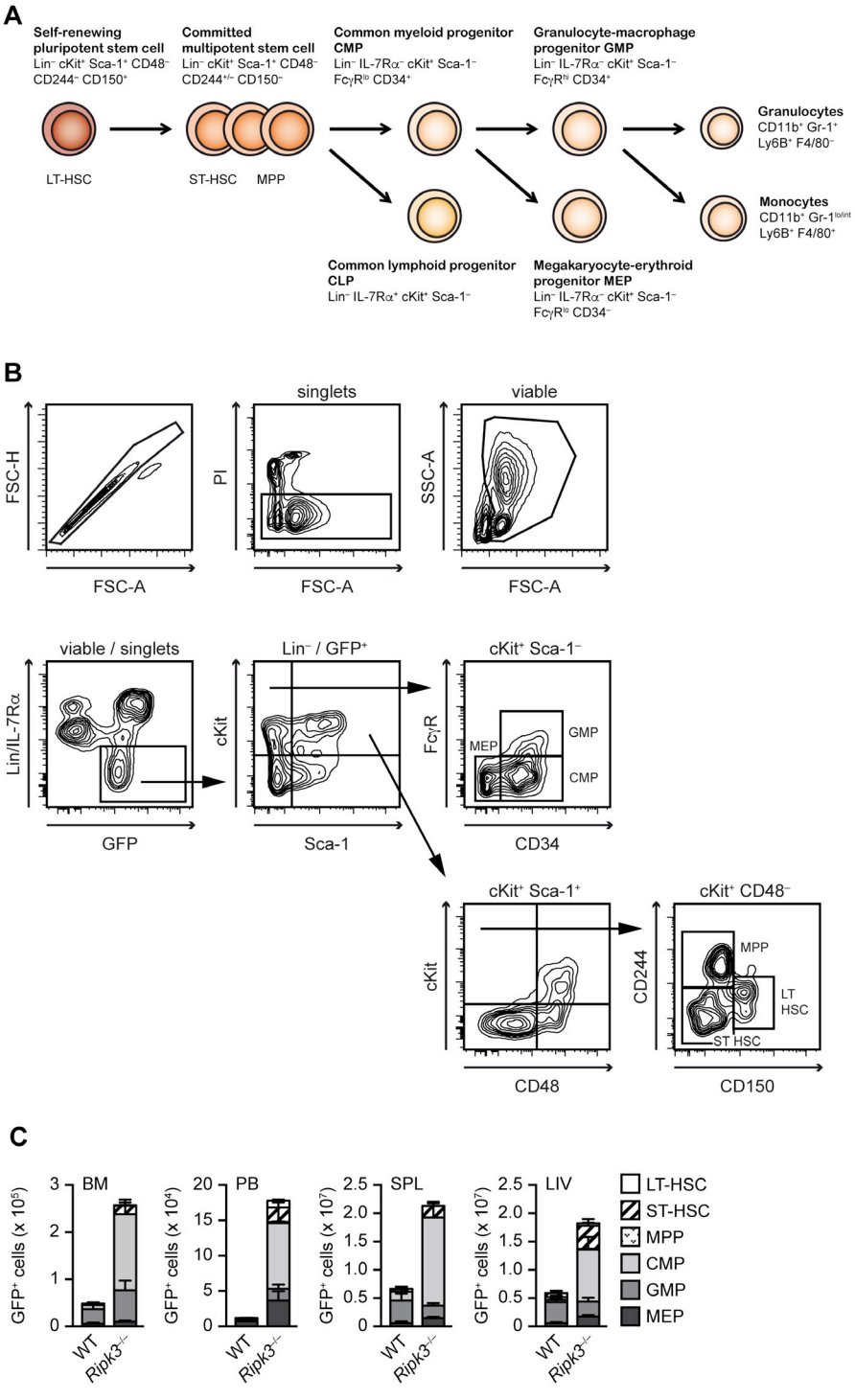

Figure S2. Gating strategy for hematopoietic stem cells and myeloid progenitor lineages. Related to Figure 2.
(A) Origins and expression of cell surface markers used to identify mouse hematopoietic stem cells and myeloid progenitor lineages as described previously (Akashi, 2000; Kiel et al., 2005). (B) Gating scheme used to determine HSPC populations. (C) Absolute numbers of HSPC subsets (LT-HSC, ST-HSC, MPP, CMP, GMP and MEP) in the BM (per hind limb), PB, SPL and LIV of primary FLT3-ITD–transplanted WT and *Ripk3*$^{-/-}$ mice in (Figure 2A). Data in (C) depict eight mice per genotype. Error bars represent mean ± SEM.

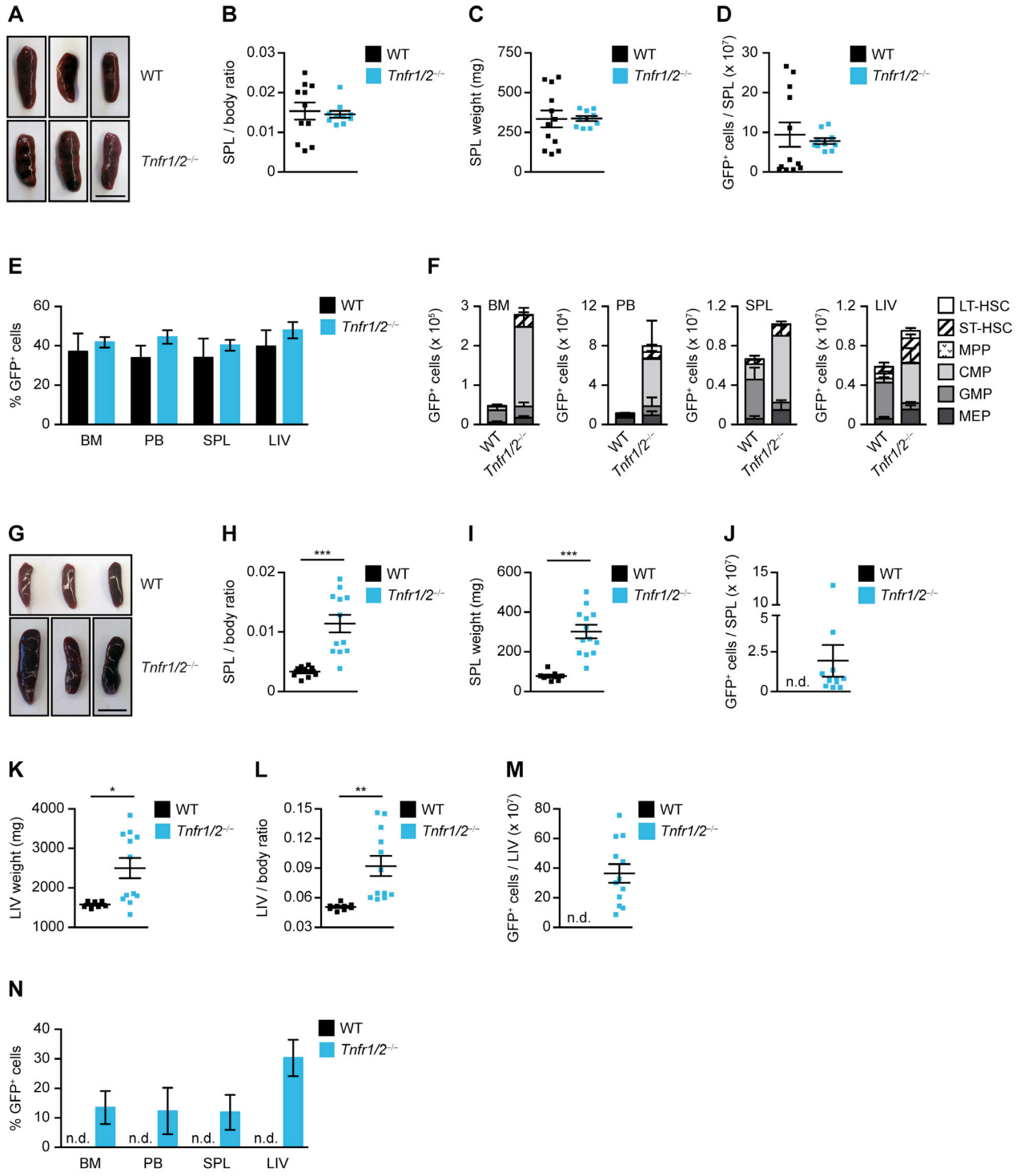

Figure S3. Increased leukemic burden in *Tnfr1/2*$^{-/-}$ FLT3-ITD. Related to Figure 3.
(A) Spleens of mice in (Figure 3A) transplanted with FLT3-ITD–transduced WT and *Tnfr1/2*$^{-/-}$ BM. Scale bar is 1 cm. (B) SPL/body ratio, (C) SPL weight and (D) absolute numbers of GFP^{+} cells/SPL from mice in (Figure 3A). (E) Frequency of GFP^{+} cells and (F) absolute numbers of HSPC subsets (LT-HSC, ST-HSC, MPP, CMP, GMP and MEP) in the BM (per hind limb), PB, SPL, and LIV from mice in (Figure 3A). Data in (B-F) depict eight mice per genotype. (G) Spleens of mice in (Figure 3F) serially transplanted with GFP^{+} splenocytes from primary FLT3-ITD–transplanted WT and *Tnfr1/2*$^{-/-}$ mice. Scale bar is 1 cm. (H) SPL/body ratio, (I) SPL weight and (J) absolute numbers of GFP^{+} cells/SPL from mice in (Figure 3F). (K) LIV/body ratio, (L) LIV weight and (M) absolute numbers of GFP^{+} cells/LIV from mice in (Figure 3F). (N) Frequency of GFP^{+} cells in the BM, PB, SPL and LIV from mice in (Figure 3F). Data in (H-N) depict nine WT and 12 *Tnfr1/2*$^{-/-}$ mice. Each dot represents a mouse and error bars represent mean ± SEM. p values Student´s t test *p<0.05, **p<0.005, ***p<0.0005.

A

Index	Term	Adjusted p value	Z score	Combined Score	Genes
1	inflammatory response (GO:0006954)	1.41E-06	-2.38	32.09	*Il10; Ciita; Ecm1; Cd40; Sema7a; Cxcl2; Aif1; Il1a; Tpst1; Il18rap; Axl; Il1b; Ccl4; Spp1; Blnk; Ccl3; Adam8; Ccr5; Mgll*
2	cellular response to cytokine stimulus (GO:0071345)	2.84E-06	-2.46	31.43	*Cd86; Cd74; Ciita; Ifitm1; Edn1; Il1r2; Csf2rb; Aif1; Il1a; Socs3; Ifng; Axl; Irf1; Il1b; Ccl3; Irf7; Gbp2; Ccr5; Jak3; Il13ra1*
5	regulation of leukocyte activation (GO:0002694)	8.96E-06	-2.51	29.12	*Il10; Cd86; Cd74; Cd40; Tnfsf14; Cdkn2a; Aif1; Dpp4; Ifng; Axl; Il1b; Irf1; Adam8; Jak3; Card11; Il13ra1; Cd276*
6	regulation of cytokine production (GO:0001817)	8.62E-06	-2.49	29.07	*Cd86; Il10; Cd74; Cd40; Sema7a; Apoa1; Mapk13; Il1a; Ifng; Axl; Il1b; Irf1; Bcl3; Irf7; Ccl3; Adam8; Jak3; Card11; Cd276*
7	positive regulation of cytokine production (GO:0001819)	8.11E-06	-2.44	28.62	*Cd86; Il10; Cd74; Cd40; Sema7a; Mapk13; Il1a; Ifng; Il1b; Irf1; Bcl3; Irf7; Ccl3; Adam8; Card11; Cd276*
10	regulation of mononuclear cell proliferation (GO:0032944)	8.73E-06	-2.39	27.83	*Cd86; Il10; Cd74; Cd40; Ifng; Cdkn2a; Il1b; Irf1; Aif1; Card11; Il13ra1; Cd276*
12	regulation of leukocyte proliferation (GO:0070663)	9.06E-06	-2.38	27.67	*Il10; Cd86; Cd74; Cd40; Ifng; Cdkn2a; Il1b; Irf1; Aif1; Card11; Il13ra1; Cd276*
28	cytokine-mediated signaling pathway (GO:0019221)	2.16E-05	-2.33	25.00	*Cd74; Ciita; Ifitm1; Il1r2; Csf2rb; Il1a; Socs3; Ifng; Il1b; Irf1; Irf7; Gbp2; Ccr5; Jak3; Il13ra1*

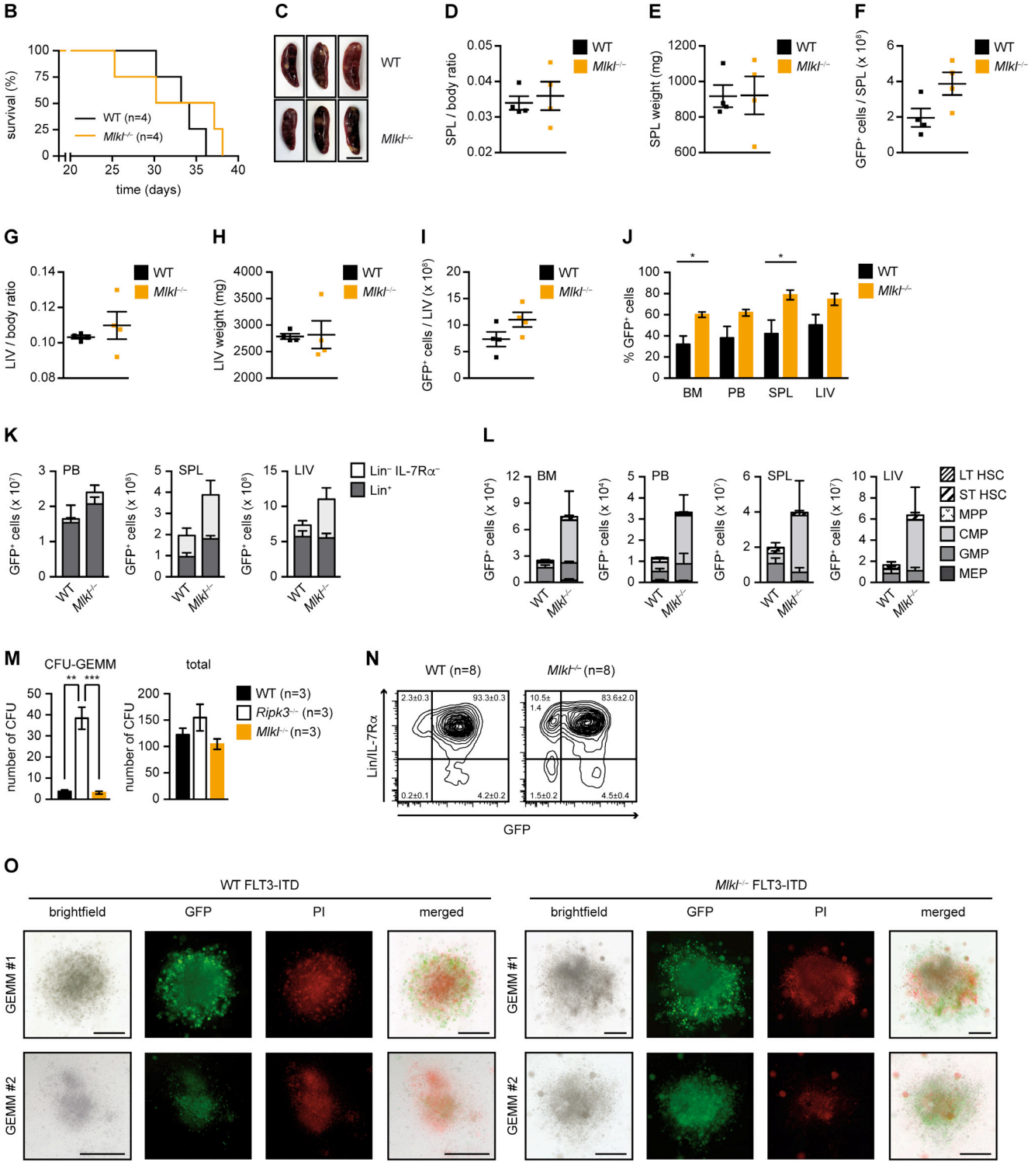

Figure S4. Leukemogenesis of *Mlkl*$^{-/-}$ FLT3-ITD. Related to Figure 4.

(A) The table shows a selection of eight inflammatory GO terms (ranked by the combined score) of the top 30 GO terms upregulated by FLT3-ITD signaling in FACS-sorted murine FLT3-ITD Lin$^-$ cells compared to empty-vector controls at 48 hr post infection. Each GO term is accompanied by the list of upregulated genes included. (B) Survival of mice transplanted with FLT3-ITD–transduced WT or *Mlkl*$^{-/-}$ BM. Median latency WT 33.5 days vs. *Mlkl*$^{-/-}$ 33.5 days. (C) Spleens of mice in (B). Scale bar is 1 cm. (D) SPL/body ratio, (E) SPL weight and (F) absolute numbers of GFP$^+$ cells/SPL from mice in (B). (G) LIV/body ratio, (H) LIV weight and (I) absolute numbers of GFP$^+$ cells/LIV from mice in (B). (J) Flow cytometric analysis to determine the frequency of GFP$^+$ cells, (K) absolute numbers of GFP$^+$ mature (Lin$^+$), HSPC (Lin$^-$ IL-7Ra$^-$) and (L) HSPC subsets (LT-HSC, ST-HSC, MPP, CMP, GMP and MEP) in the BM (per hind limb), PB, SPL and LIV from mice in (B). Data in (B-L) represent one experiment with four mice per genotype. (M) Colony count of FLT3-ITD–transduced WT and *Mlkl*$^{-/-}$ BM. Data are representative of two independent experiments. (N) Flow cytometric analysis of in vitro cultures of FLT3-ITD–transduced WT and *Mlkl*$^{-/-}$ BM. Numbers in plots indicate percentage (± SEM). Data represent one experiment with eight mice per genotype. (O) Fluorescence microscopic analyses of GFP expression and propidium iodide (PI) staining in CFU-GEMM of FLT3-ITD−transduced WT and *Mlkl*$^{-/-}$ BM. Scale bar is 500 µm. Data are representative of two independent experiments and at least six mice per genotype. Each dot represents a mouse and error bars represent mean ± SEM. p values (B) Mantel Cox test otherwise Student´s t test *$p<0.05$, **$p<0.005$, ***$p<0.0005$.

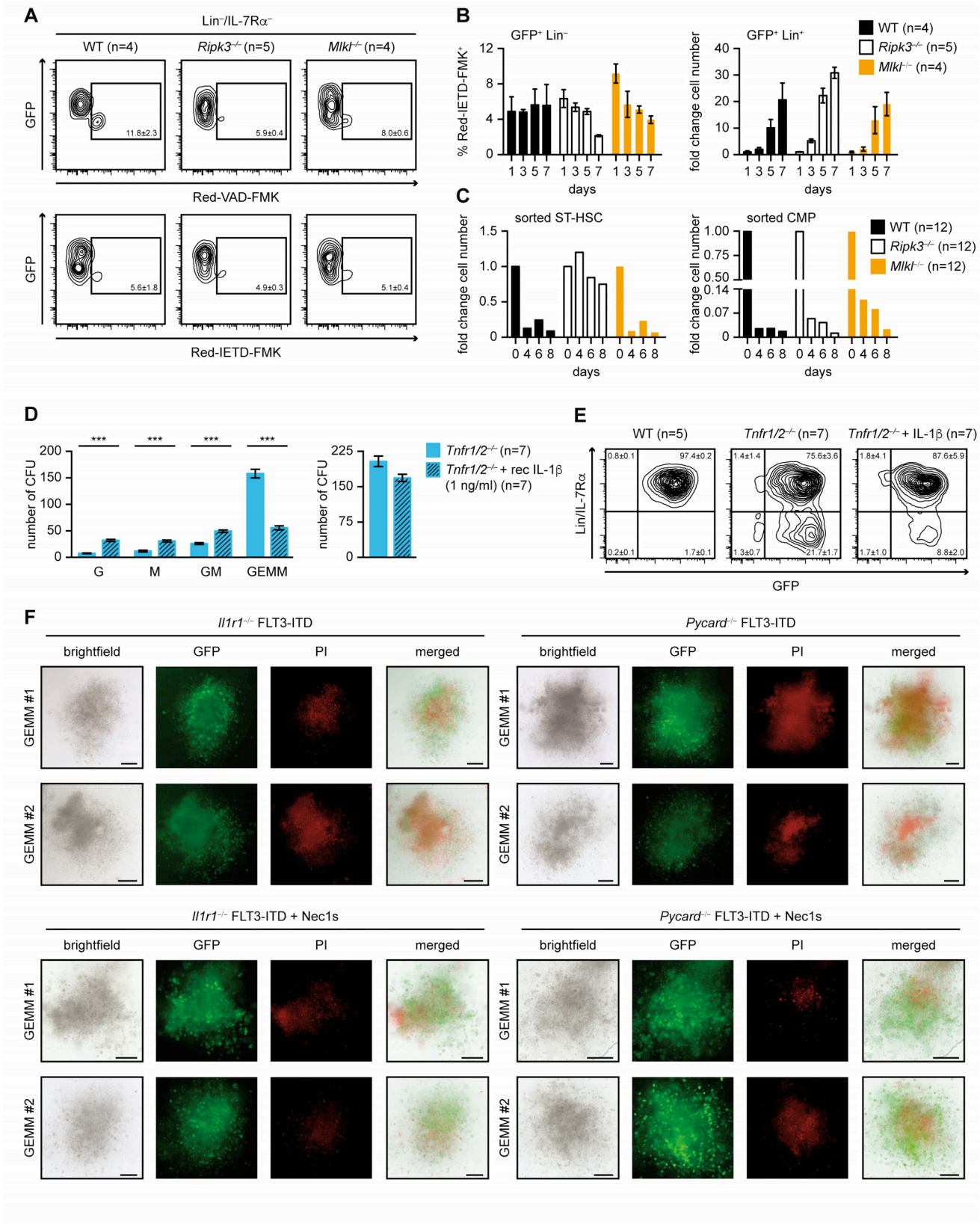

Figure S5. Caspase activation and cell death in FLT3-ITD transduced BM. Related to Figure 5.
(A) Representative flow-cytometry analysis (day 5) of Red-VAD-FMK and Red-IETD-FMK staining in GFP$^+$Lin$^-$ FLT3-ITD–transduced WT, *Ripk3*$^{-/-}$ and *Mlkl*$^{-/-}$ BM cells. Numbers indicate percentage (± SEM). (B) Red-IETD-FMK staining in FLT3-ITD–transduced GFP$^+$Lin$^-$ cells and fold change of GFP$^+$Lin$^+$ cell numbers of WT, *Ripk3*$^{-/-}$ and *Mlkl*$^{-/-}$ BM cells over time. Data represent one experiment. (C) Fold change of FLT3-ITD–transduced sorted ST-HSC and CMP cell numbers over time from WT, *Ripk3*$^{-/-}$ and *Mlkl*$^{-/-}$. Data representat one experiment. (D) Colony count of FLT3-ITD–transduced *Tnfr1/2*$^{-/-}$ BM cultured in the presence or absence of recombinant mouse IL-1β (1 ng/ml). Data represent two independent experiments. (E) Flow cytometric analysis of FLT3-ITD–transduced WT and *Tnfr1/2*$^{-/-}$ BM cultured in the presence or absence of recombinant mouse IL-1β (1 ng/ml). Numbers in plots indicate percentage (± SEM). Data represent one experiment. (F) Fluorescence microscopic analyses of GFP expression and propidium iodide (PI) staining in CFU-GEMM of FLT3-ITD−transduced *Il1r1*$^{-/-}$ and *Pycard*$^{-/-}$ BM (+/- Nec1s). Scale bar is 300 µm. Data are representative of two experiments. Error bars represent mean ± SEM. p values Student´s t test ***p<0.0005.

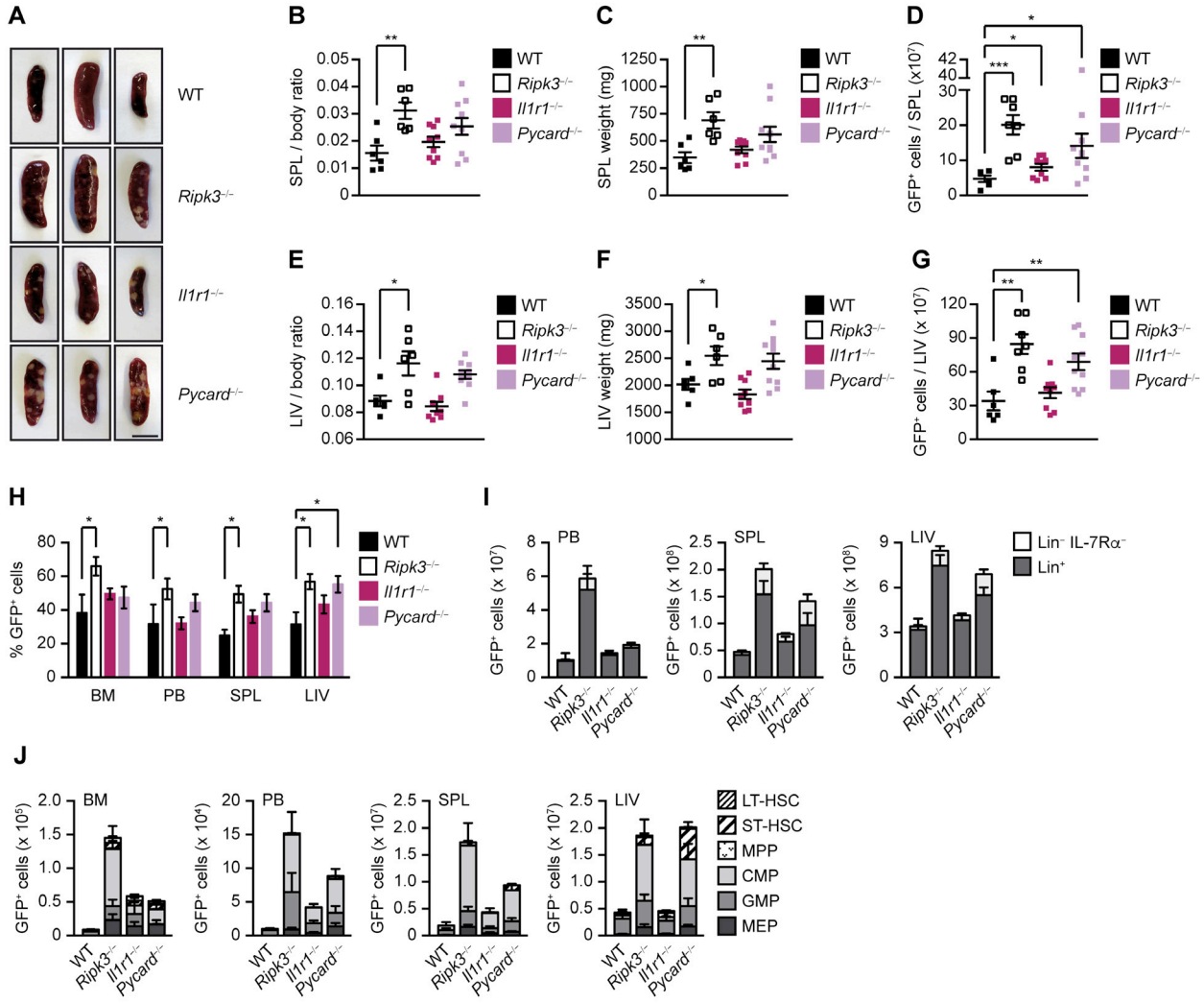

Figure S6. Leukemic burden of *Pycard*$^{-/-}$ FLT3-ITD and *Il1r1*$^{-/-}$ FLT3-ITD mice and inhibition of cell death by Nec1s. Related to Figure 6.

(A) Spleens of mice in (Figure 6A) transplanted with FLT3-ITD–transduced WT, *Ripk3*$^{-/-}$, *Il1r1*$^{-/-}$ or *Pycard*$^{-/-}$ BM. Scale bar is 1 cm. (B) SPL/body ratio, (C) SPL weight and (D) absolute numbers of GFP^{+} cells/SPL from mice in (Figure 6A). (E) LIV/body ratio, (F) LIV weight and (G) absolute numbers of GFP^{+} cells/LIV from mice in (Figure 6A). (H) Flow cytometric analysis to determine the frequency of GFP^{+} cells, (I) absolute numbers of GFP^{+} mature (Lin^{+}) cells, HSPC (Lin^{-}IL-7Rα^{-}) and (J) HSPC subsets (LT-HSC, ST-HSC, MPP, CMP, GMP and MEP) in the BM (per hind limb), PB, SPL and LIV from mice in (Figure 6A). Data represent one experiment with six WT, seven *Ripk3*$^{-/-}$, nine *Il1r1*$^{-/-}$ and ten *Pycard*$^{-/-}$ mice. Each dot represents a mouse and error bars represent mean ± SEM. p values Student´s t test *p<0.05, **p<0.005.

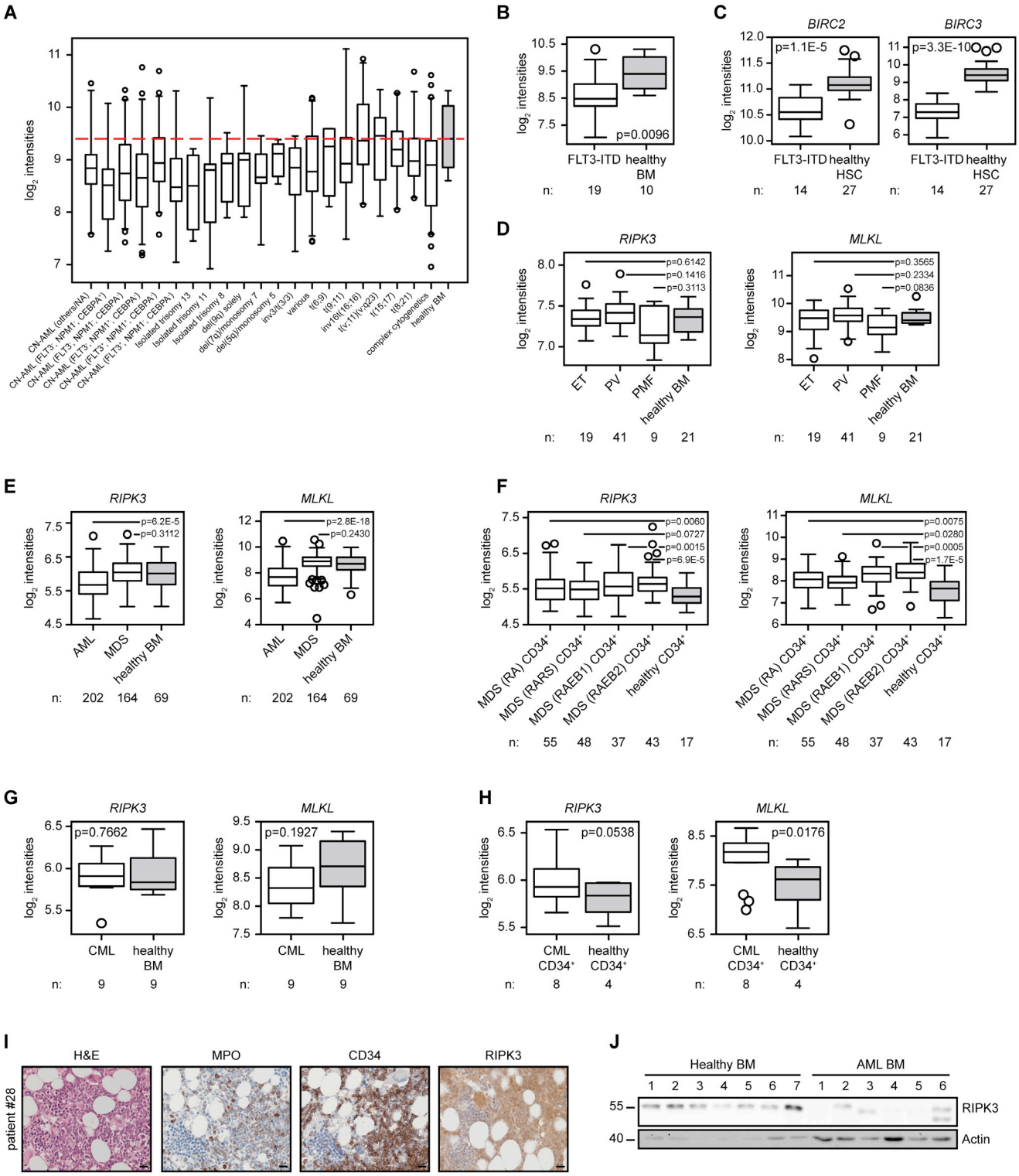

Figure S7. Reduced expression of *MLKL* in patients diagnosed with FLT3-ITD–mutated AML as well as several additional AML subtypes. Related to Figure 7.

(A) Gene expression profiles (GEP) for *MLKL* obtained from 562 de novo AML patient samples and 10 healthy BM controls (GEO: GSE37642). AML subtypes are defined by standardized cytogenetic or molecular genetic aberrations. Mean expression of *MLKL* in healthy controls is indicated by the red dashed line. (B) GEP for *MLKL* in cytogenetically normal FLT3-ITD–mutated AML samples (GEO: GSE37642). (C) GEP for *BIRC2* and *BIRC3* in cytogenetically normal FLT3-ITD–mutated AML samples (GEO: GSE6891). (D) GEP for *RIPK3* and *MLKL* in BCR-ABL–negative myeloproliferative neoplasms (MPN) samples: essential thrombocythemia (ET), polycythemia vera (PV), and primary myelofibrosis (PMF) (GEO: GSE26049). (E) Profiles for *RIPK3* and *MLKL* in AML and myelodysplastic syndromes (MDS) samples (GEO: GSE15061). (F) Profiles for *RIPK3* and *MLKL* in MDS samples (GEO: GSE19429). (G) Profiles for *RIPK3* and *MLKL* in BCR-ABL–positive chronic myeloid leukemia (CML) samples (GEO: GSE33075). (H) Profiles for *RIPK3* and *MLKL* in BCR-ABL–positive CML samples (GEO: GSE24739). Data in (A-H) are depicted as Tukey boxplots, depicting the median, the upper and lower quartile and whiskers with maximum 1.5 interquartile range. Outliers are plotted as individual points. In (A-H) n = number of patients per cohort. (I) H&E and IHC images of BM biopsies from one patient with de novo AML without *FLT3* or *NPM1* mutation stained for MPO, CD34 or RIPK3 (brown) and counterstained with hematoxylin (blue). Scale bar is 20 µm. Infiltration rate is 80%. (J) Immunoblot of healthy bulk BM and AML BM patient samples for RIPK3. p values Student´s t test.

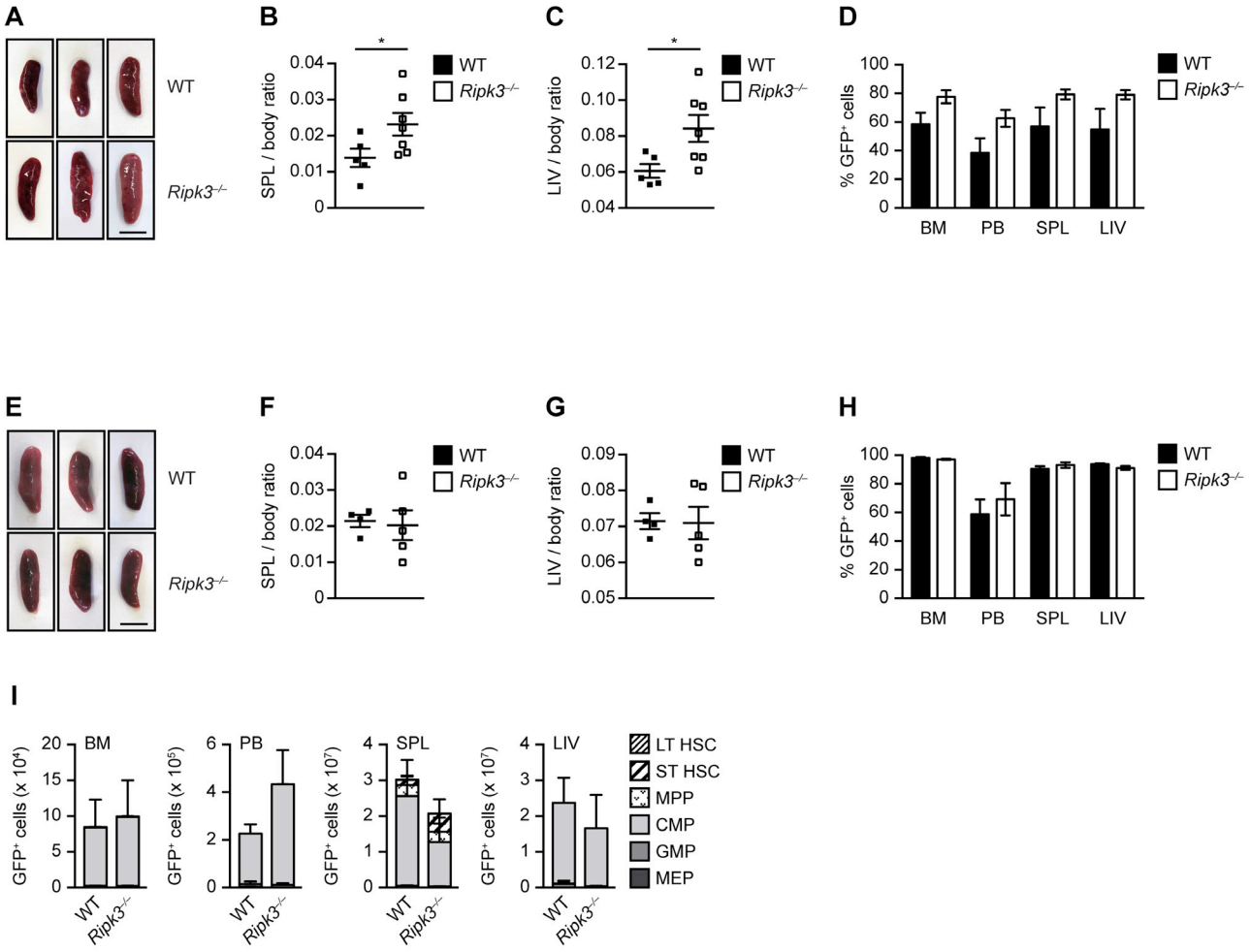

Figure S8. Suppression of RIPK3 accelerates leukemogenesis driven by t(8;21) but not by MLL-translocated MLL-ENL AML. Related to Figure 8.

(A) Spleens of mice in (Figure 8B) transplanted with AML1-ETO9a–transduced WT and *Ripk3*$^{-/-}$ BM. Scale bar is 1 cm. (B) SPL/body ratio and (C) LIV/body ratio from mice in (Figure 8B). (D) Frequency of GFP^{+} cells from mice in (Figure 8B). In (B-D) data depict five WT and seven *Ripk3*$^{-/-}$ mice. (E) Spleens of mice (in Figure 8H) transplanted with MLL-ENL–transduced WT and *Ripk3*$^{-/-}$ BM. Scale bar is 1 cm. (F) SPL/body ratio and (G) LIV/body ratio from mice in (Figure 8H). (H) Frequency of GFP^{+} cells and (I) absolute numbers of HSPC subsets (LT-HSC, ST-HSC, MPP, CMP, GMP and MEP) in the BM (per hind limb), PB, SPL and LIV from mice in (Figure 8H). In (F-I) data depict five WT and five *Ripk3*$^{-/-}$ mice. Each dot represents a mouse and error bars represent mean ± SEM. p values Student´s t test *p<0.05.

Supplemental Experimental Procedures

DNA constructs and retrovirus preparation

The FLT3-ITD, MLL-ENL/neo, and AML1-ETO9a (Addgene plasmid 12433) retroviral constructs have been previously described (Glaser et al., 2012; Grundler et al., 2005). Retrovirus supernatants were produced in the ecotropic packaging cell line Phoenix-E (G. Nolan, Stanford, CA) by calcium-phosphate transfection. pMIG served as a control.

Transduction and transplantation of murine bone marrow

Bone marrow was harvested from C57BL/6 donor mice of indicated genotypes 4 days after injection of 150 mg/kg 5-fluorouracil (5-FU; medac) and pre-stimulated overnight in RPMI/20% FCS supplemented with growth factors (10 ng/ml IL-3, 10 ng/ml IL-6; R&D Systems, 100 ng/ml SCF; eBioscience). Cells were transduced by two rounds of spin infection (1200 g, 32°C, 90 min) every 24 hr in retroviral supernatant supplemented with growth factors and 4 µg/ml polybrene (Millipore). Subsequently, cells were resuspended in PBS (Sigma) and injected i.v. into lethally irradiated (9 Gy) C57BL/6 WT recipient mice. Mice with disease were sacrificed. Peripheral blood white blood cell counts (WBC) were measured by scil Vet abc (scil animal care company).

For serial transplantations, C57BL/6 WT recipient mice were subjected sub-lethally irradiated with a single dose of 4.5 Gy. In experiments using *Il1r1*$^{-/-}$ and *Pycard*$^{-/-}$ BM all recipient mice (including recipients of WT and *Ripk3*$^{-/-}$ BM) were co-transplanted with unchallenged WT BM to prevent engraftment failure of the *Il1r1*$^{-/-}$ BM, as has been previously reported (Orelio et al., 2009).

Progenitor cell analysis

For flow cytometry and RNA expression analysis FLT3-ITD–transduced BM cells were cultured in RPMI/10% FCS for 7 days in the absence of cytokines. For colony forming cell assays, all duplicate cultures were performed in 35 mm petri dishes in murine methylcellulose medium (Methocult, Stem Cell Technologies). BM cells of unchallenged or 5-FU–challenged mice were plated in M3434 medium at a density of $5x10^4$ cells/plate. FLT3-ITD–infected BM cells were plated in M3234 medium at a density of $1x10^4$ cells/plate in the presence of the following cytokines and inhibitors if indicated: IL-1β (1 ng/ml; R&D Systems), Nec1s (30 µM), Z-YVAD-FMK (YVAD)(10 µM; BioVision), IETD (10 µM; BD Biosciences), and Anakinra (15 µg/ml; Sobi). Colonies were counted after 10 days by light microscopy. Empty vector-infected cells were used as negative controls and did not yield any colony formation.

For analysis of colony forming units (CFU) cell viability, colonies were grown for 10 days in the presence of propidium iodide (PI) (0.8 µg/ml; Sigma) and representative CFU-GEMM were imaged using a Keyence BZ-9000 (Biorevo) fluorescence microscope.

For colony forming cell assays of FLT3-ITD–transduced ST-HSC and CMP, cells were sorted based on GFP and surface marker expression as described in (Figure S2B). 1000 cells were plated in M3234 medium as duplicate cultures and analyzed as described above. For flow cytometry ST-HSC and CMP were cultured in RPMI/10% FCS for 8 days in the absence of cytokines

For measuring cytokines from colony forming cell assays, cultures were washed off with PBS and cells removed by centrifugation. Supernatants were concentrated with Vivaspin 10 kDa filters (Sartorius) and cytokines were quantified using Cytometric Bead Array (CBA; BD Biosciences) according to the manufacturer's instructions.

For mRNA expression RNA from in vitro cultures of FLT3-ITD–transduced BM and 5-FU–treated BM was extracted using Nucleospin®RNA (MACHEREY-NAGEL) and RNA was transcribed to cDNA with *S*uperScript II Reverse Transcriptase (Life Technologies). Primers for *Pycard, Casp1, Tnf, Il6, Ripk1*, *Mlkl* and *Il1b* are listed below. Gene expression is expressed relative to *Tbp1*. RT-PCR was performed using GoTaq® qPCR Master Mix (Promega) on a LightCycler® 480 (Roche). Experimental groups consisted of 4-9 mice and RT-PCR was performed with three technical replicates per biological replicate.

For measuring caspase activation from in vitro cultures of FLT3-ITD–transduced BM, cells were stained with lineage markers and CaspGLOW™ Red Active Caspase Staining Kit (BioVision) or CaspGLOW™ Red Active Caspase-8 Staining Kit (BioVision) according to the manufacturer's instructions and analyzed by flow cytometry.

Flow cytometric immunophenotyping

Single-cell suspensions of indicated tissue samples were prepared and red blood cells of peripheral blood were lysed before analysis. Cells were pre-incubated with Fc-block and subsequently stained with fluorescently labeled antibodies as listed below. Dead cells were excluded by PI staining. Flow analysis was performed on a BD FACS Canto II (BD Biosciences) and data were analyzed using FlowJo software (Tree Star).

Analysis of expression profiles of patient cohort datasets

Gene expression was analyzed by Affymetrix HG U133 Plus 2.0 and the HG U133A+B Set. The microarray data have been previously published (Affer et al., 2011; Benito et al., 2012; Herold et al., 2014; Mills et al., 2009; Pang et al., 2011; Pellagatti et al., 2010; Skov et al., 2011; Verhaak et al., 2009) and were retrieved from the Gene Expression Omnibus (GEO) as raw data files (GEO: GSE24739, GSE33075, GSE37642, GSE15061, GSE32719, GSE19429, GSE26049, GSE6891). For GEO accessions GSE6891 and GSE32719 quality control was carried out as described previously (Valk et al., 2004) and samples were analyzed as one dataset. For probes to probe set annotation custom chip definition files (CDFs) were used based on GeneAnnot version 2.0, synchronized with GeneCards Version 3.04. These CDFs decrease the total number of probe sets (one probe set per gene), and potentially increase the specificity of the analyses by eliminating cross-hybridizing probes (probes are restricted by sequence specificity). Data normalization was performed using the Robust Multichip Average (RMA) method as described previously (Irizarry et al., 2003). Some probe sets on the A+B chips tend to have lower mean signal levels and higher standard deviations than the corresponding probe sets on the Plus 2.0 chips. To eliminate this batch effect resulting from

the different chip designs, a second normalization using an empirical Bayesian method was performed for samples from GEO: GSE37642 as reported previously (Herold et al., 2014).

RNA Isolation and Analysis

Total RNA isolation was performed from FACS-sorted Lin^- GFP^+ populations of WT BM transduced with FLT3-ITD or empty vector control 48 hr after infection using the Absolutely RNA Microprep Kit (Agilent Technologies) according to the manufacturer's instructions. The quality of total RNA was checked by gel analysis using the total RNA Nano chip assay on an Agilent 2100 Bioanalyzer (Agilent Technologies). Only samples with RNA index values greater than 8.5 were selected for expression profiling. RNA concentrations were determined using the NanoDrop spectrophotometer (NanoDrop Technologies).

Probe Labeling and Illumina Sentrix BeadChip array Hybridization

Biotin-labeled cRNA samples for hybridization on Illumina Mouse Sentrix-8 v2 BeadChip arrays (Illumina, Inc.) were prepared according to Illumina's recommended sample labeling procedure based on the modified Eberwine protocol (Eberwine et al., 1992). In brief, 250 ng total RNA was used for complementary DNA (cDNA) synthesis, followed by an amplification/labeling step (in vitro transcription) to synthesize biotin-labeled cRNA according to the MessageAmp II aRNA Amplification kit (Ambion, Inc.). Biotin-16-UTP was purchased from Roche Applied Science. The cRNA was column purified according to TotalPrep RNA Amplification Kit, and eluted in 60 µl of water. Quality of cRNA was controlled using the RNA Nano Chip Assay on an Agilent 2100 Bioanalyzer and spectrophotometrically quantified (NanoDrop).

Hybridization was performed at 58°C, in GEX-HCB buffer (Illumina Inc.) at a concentration of 100 ng cRNA/µl, unsealed in a wet chamber for 20 h. Spike-in controls for low, medium and highly abundant RNAs were added, as well as mismatch control and biotinylation control oligonucleotides. Microarrays were washed once in High Temp Wash buffer (Illumina Inc.) at 55°C and then twice in E1BC buffer (Illumina Inc.) at room temperature for 5 min (in between washed with ethanol at room temperature). After blocking for 5 min in 4 ml of 1% (w/v%) Blocker Casein in phosphate buffered saline Hammarsten grade (Pierce Biotechnology, Inc.), array signals are developed by a 10 min incubation in 2 ml of 1 µg/ml Cy3-streptavidin (Amersham Biosciences) solution and 1% blocking solution. After a final wash in E1BC, the arrays were dried and scanned.

Scanning and data analysis

Microarray scanning was done using a Beadstation array scanner, setting adjusted to a scaling factor of 1 and PMT settings at 430. Data extraction was done for all beads individually, and outliers are removed when >2.5 MAD (median absolute deviation). All remaining data points are used for the calculation of the mean average signal for a given probe, and standard deviation for each probe was calculated.

Data analysis was done by normalization of the signals using the quantile normalization algorithm without background subtraction, and differentially regulated genes are defined by calculating the standard deviation differences of a given probe in a one-by-one comparisons of samples or groups. As test for significance the student's t-test is used on the bead expression values of the two groups of interest. In the case of significance of expression against background we tested for greater than all negative beads for this sample and in the case of comparing separate groups we tested for inequality of the means of the groups. In both cases Benjamini-Hochberg correction was applied to the complete set of p values of all 48107 ProbeIDs on the chip. The average expression value is calculated as mean of the measured expressions of beads together with the standard deviation of the beads.

Differential gene expression was detected with limma (Ritchie et al., 2015) and only genes with adjusted $p<0.05$ and an absolute $\log_2$ fold change >0.8 were considered to be differentially expressed. Gene Ontology (GO) enrichment analysis was performed using EnrichR (Chen et al., 2013) and results with an FDR<0.05 were considered significant. All analysis steps for processing the array, detecting differential expression, and generating the heatmap were conducted with R 3.2.3 (Team, 2008).

Immunohistochemistry of human primary AML samples

For immunohistochemistry (IHC) we made use of 65 de novo AML cases at the time of diagnosis, collected between 2004 and 2015 at the institutes of pathology of the Technical University (Munich) (n=39), Ludwig-Maximilians-University (Munich) (n=20) and the Hannover Medical School (n=6) for which sufficient patient material was available. Eligible patients had received a diagnosis of de novo AML, which had been confirmed by means of a cytologic examination of blood and BM. Cases were re-evaluated using hematoxylin and eosin (HE), Giemsa, AS-D chloroacetate esterase and standard diagnostic IHC (CD34, CD117, MPO). Infiltration rate of AML blasts was >50% in most cases. 15 reactive BM biopsies from patients without AML or MPN were included as controls. Biopsies were fixed in 4% formaldehyde, EDTA decalcified, and paraffin embedded. IHC was performed using an automated immunostainer with the VIEW DAB detection kit (Ventana Medical System, Roche) according to the company's protocols for open procedures. Biopsies were stained with anti-RIPK3 (780115, R&D systems) according to the manufacturer's instructions and counterstained with hematoxylin. Appropriate positive controls were used to confirm the adequacy of the staining. Specific RIPK3 staining was localized to the cytoplasm. Human BM samples were collected according to the institutional guidelines and written informed consent was obtained from all patients in accordance with the Declaration of Helsinki. All use of patient material was approved by the Local Ethics Committees.

Immunoblotting of murine and human samples

Protein lysates were prepared by lysing cells in RIPA buffer supplemented with Complete Protease Inhibitor Cocktail (Roche), and protein phosphatase inhibitors Sodium Orthovanadate and sodium fluoride (Sigma-Aldrich) on ice. Protein concentrations of lysates were measured with Pierce BCA Protein Assay (Thermo Scientific) and 15 µg of total protein/sample in Laemmli sample buffer was loaded and separated on 12% SDS-PAGE gels, and then transferred to Nitrocellulose membranes (GE Healthcare). For detection of murine proteins the following antibodies were used: RIPK3 (ADI-905-242-100, ENZO), Pan-

specific cIAP1/2 (315301, R&D Systems), XIAP (610716, BD Bioscience), MLKL (3H1, Millipore), IL-1β (AB-401-NA, R&D Systems), caspase-1 (Casper-1, Adipogen), PYCARD (AL177, Adipogen), and Actin (13E5, Cell Signaling). Human RIPK3 was detected with anti-RIPK3 (780115, R&D systems). Secondary HRP-conjugated antibodies were from Jackson ImmunoResearch Inc. Chemiluminescence was detected using Pierce ECL Plus Substrate (Thermo Scientific) and a ChemoCam Imager (INTAS).

Primers used to perform RT-PCR analysis

Gene	Primer direction	Primer sequence (5'->3')	Reference
Pycard	Forward	GAGCAGCTGCAAACGACTAA	
	Reverse	GCTGGTCCACAAAGTGTCCT	
Casp1	Forward	AGGAATTCTGGAGCTTCAATCAG	
	Reverse	TGGAAATGTGCCATCTTCTTT	
Tnf	Forward	CCACGCTCTTCTGTCTACTGA AC	
	Reverse	TTGTCACTCGAATTTTGAGAAGATG	
Il1b	Forward	TGTAATGAAAGACGGCACACC	
	Reverse	TCTTCTTTGGGTATTGCTTGG	
Ripk3	Forward	GCCTTCCTCTCAGTCCACAC	
	Reverse	ACGCACCAGTAGGCCATAAC	
Il6	Forward	CAGGATACCACTCCCAACAGACC	Nenci et al., 2007
	Reverse	AAGTGCATCATCGTTGTTCATACA	
Mlkl	Forward	GGATTGCCCTGAGTTGTTGC	Kaiser et al., 2013
	Reverse	AACCGCAGACAGTCTCTCCA	
Birc2	Forward	TGCCTGTGGTGGGAAACTGA	Owens et al., 2010
	Reverse	GCTCGGGTGAACAGGAACA	
Birc3	Forward	TATTTGTGCAACAGGACATTAGGAGT	Owens et al., 2010
	Reverse	CACA TTCTTTCCTCCTGGAGTTTC	
Tbp1	Forward	CCACCAGCAGTTCAGTAGCTATGA	
	Reverse	TGCTCTAACTTTAGCACCTGTTAATACAAC	

Antibodies used to separate mouse hematopoietic cell subsets

Population	Surface marker
lymphoid	CD19 (eBio1D3), TCR-b (H57-597), CD4 (Gk1.5), CD8a (53–6.7).
myeloid	CD11b (M1/70), F4/80 (BM8), Gr-1 (RB6-8C5), Ly6B.2 (AbD Serotec)
HSPC	Sca-1 (D7), c-Kit (2B8), CD34 (700011; R&D Systems), CD16/32 (93), CD244.2 (eBio244F4), CD150 (mShad150), CD48 (HM48-1)
Lineage markers	IL-7Ra (A7R34), B220 (RA3_6B2), CD19 (eBio1D3), TCR-b (H57-597), CD3 (17A2), CD11b (M1/70), Gr-1 (RB6-8C5), Ly6C (HK1.4), TER-119 (TER-119

If not otherwise stated, Fc-block and all antibodies were purchased from eBioscience.

Supplemental References

Affer, M., Dao, S., Liu, C., Olshen, A. B., Mo, Q., Viale, A., Lambek, C. L., Marr, T. G., and Clarkson, B. D. (2011). Gene Expression Differences between Enriched Normal and Chronic Myelogenous Leukemia Quiescent Stem/Progenitor Cells and Correlations with Biological Abnormalities. J Oncol *2011*, 798592.

Akashi, K., Traver, D., Miyamoto, T., and Weissman, I. L. (2000). A clonogenic common myeloid progenitor that gives rise to all myeloid lineages. Nature *404*, 193-197.

Benito, R., Lumbreras, E., Abáigar, M., Gutiérrez, N. C., Delgado, M., Robledo, C., García, J. L., Rodríguez-Vicente, A. E., Cañizo, M. C., and Rivas, J. M. H. (2012). Imatinib therapy of chronic myeloid leukemia restores the expression levels of key genes for DNA damage and cell-cycle progression. Pharmacogenetics and Genomics *22*, 381-388.

Chen, E. Y., Tan, C. M., Kou, Y., Duan, Q., Wang, Z., Meirelles, G. V., Clark, N. R., and Ma'ayan, A. (2013). Enrichr: interactive and collaborative HTML5 gene list enrichment analysis tool. BMC Bioinformatics *14*, 128.

Eberwine, J., Yeh, H., Miyashiro, K., Cao, Y., Nair, S., Finnell, R., Zettel, M., and Coleman, P. (1992). Analysis of gene expression in single live neurons. Proc Natl Acad Sci U S A *89*, 3010-3014.

Glaser, S. P., Lee, E. F., Trounson, E., Bouillet, P., Wei, A., Fairlie, W. D., Izon, D. J., Zuber, J., Rappaport, A. R., Herold, M. J.*, et al.* (2012). Anti-apoptotic Mcl-1 is essential for the development and sustained growth of acute myeloid leukemia. Genes Dev *26*, 120-125.

Grundler, R., Miething, C., Thiede, C., Peschel, C., and Duyster, J. (2005). FLT3-ITD and tyrosine kinase domain mutants induce 2 distinct phenotypes in a murine bone marrow transplantation model. Blood *105*, 4792-4799.

Irizarry, R. A., Hobbs, B., Collin, F., Beazer-Barclay, Y. D., Antonellis, K. J., Scherf, U., and Speed, T. P. (2003). Exploration, normalization, and summaries of high density oligonucleotide array probe level data. Biostatistics *4*, 249-264.

Kaiser, W. J., Sridharan, H., Huang, C., Mandal, P., Upton, J. W., Gough, P. J., Sehon, C. A., Marquis, R. W., Bertin, J., and Mocarski, E. S. (2013). Toll-like receptor 3-mediated necrosis via TRIF, RIP3, and MLKL. J Biol Chem *288*, 31268-31279.

Mills, K. I., Kohlmann, A., Williams, P. M., Wieczorek, L., Liu, W. M., Li, R., Wei, W., Bowen, D. T., Loeffler, H., Hernandez, J. M.*, et al.* (2009). Microarray-based classifiers and prognosis models identify subgroups with distinct clinical outcomes and high risk of AML transformation of myelodysplastic syndrome. Blood *114*, 1063-1072.

Nenci, A., Becker, C., Wullaert, A., Gareus, R., van Loo, G., Danese, S., Huth, M., Nikolaev, A., Neufert, C., Madison, B.*, et al.* (2007). Epithelial NEMO links innate immunity to chronic intestinal inflammation. Nature *446*, 557-561.

Orelio, C., Peeters, M., Haak, E., van der Horn, K., and Dzierzak, E. (2009). Interleukin-1 regulates hematopoietic progenitor and stem cells in the midgestation mouse fetal liver. Haematologica *94*, 462-469.

Owens, T. W., Foster, F. M., Tanianis-Hughes, J., Cheung, J. Y., Brackenbury, L., and Streuli, C. H. (2010). Analysis of inhibitor of apoptosis protein family expression during mammary gland development. BMC Dev Biol *10*, 71.

Pang, W. W., Price, E. A., Sahoo, D., Beerman, I., Maloney, W. J., Rossi, D. J., Schrier, S. L., and Weissman, I. L. (2011). Human bone marrow hematopoietic stem cells are increased in frequency and myeloid-biased with age. Proc Natl Acad Sci U S A *108*, 20012-20017.

Pellagatti, A., Cazzola, M., Giagounidis, A., Perry, J., Malcovati, L., Della Porta, M. G., Jadersten, M., Killick, S., Verma, A., Norbury, C. J.*, et al.* (2010). Deregulated gene expression pathways in myelodysplastic syndrome hematopoietic stem cells. Leukemia *24*, 756-764.

Ritchie, M. E., Phipson, B., Wu, D., Hu, Y., Law, C. W., Shi, W., and Smyth, G. K. (2015). limma powers differential expression analyses for RNA-sequencing and microarray studies. Nucleic Acids Res *43*, e47.

Skov, V., Larsen, T. S., Thomassen, M., Riley, C. H., Jensen, M. K., Bjerrum, O. W., Kruse, T. A., and Hasselbalch, H. C. (2011). Whole-blood transcriptional profiling of interferon-inducible genes identifies highly upregulated IFI27 in primary myelofibrosis. Eur J Haematol *87*, 54-60.

Team, R. D. C. (2008). R: A Language and Environment for Statistical Computing. R Foundation for Statistical Computing,Vienna, Austria.

Valk, P. J., Verhaak, R. G., Beijen, M. A., Erpelinck, C. A., Barjesteh van Waalwijk van Doorn-Khosrovani, S., Boer, J. M., Beverloo, H. B., Moorhouse, M. J., van der Spek, P. J., Lowenberg, B., and Delwel, R. (2004). Prognostically useful gene-expression profiles in acute myeloid leukemia. N Engl J Med *350*, 1617-1628.